






# Production and enhancement of (multi-) strange hadrons in Au + Au collisions at $\sqrt{s_{NN}} = 200$ GeV RHIC energy and Pb + Pb collisions at $\sqrt{s_{NN}} = 2.76$ TeV LHC energy

Arpit Singh <sup>1,\*</sup>, P. K. Srivastava <sup>2,†</sup>, Gauri Devi <sup>1,‡</sup> and B. K. Singh <sup>1,§</sup>

<sup>1</sup>Department of Physics, Institute of Science, Banaras Hindu University, Varanasi-221005, India

<sup>2</sup>Physics and Material Science Department, Madan Mohan Malviya University of Technology, Gorakhpur-273015, India

 (Received 23 August 2021; revised 24 August 2022; accepted 9 December 2022; published 8 February 2023)

In this article, we investigate Au + Au and Pb + Pb collision systems to understand the (multi-) strange hadron production at Relativistic Heavy Ion Collider (RHIC) and Large Hadron Collider (LHC) energies using the Monte Carlo HYDJET++ model. We study the  $p_T$  spectra, particle ratios, and strangeness enhancement factor for (multi-) strange hadrons. The  $p_T$  spectra of  $K^+(K^-)$ ,  $K_S^0$ ,  $\Lambda(\bar{\Lambda})$ ,  $\Xi^-(\bar{\Xi}^+)$ , and  $\Omega^-(\bar{\Omega}^+)$  are shown for both Au + Au and Pb + Pb collision systems in various centrality intervals. We find that the strange quark thermalization might not be achieved by the model for multistrange baryons toward peripheral collisions. The  $p_T$ -differential particle ratios, focused on strange hadron-to-meson ratios, are reported for 0–5% and 40–60% centrality intervals for both the collision systems. We observe an enhancement in the particle ratios at intermediate  $p_T$  region.  $p_T$  integrated strange-to-nonstrange ratios suggest that chemical equilibrium might not be achieved for multistrange hadrons. We report the strangeness enhancement factor for  $\Lambda(\bar{\Lambda})$ ,  $\Xi^-(\bar{\Xi}^+)$ , and  $\Omega^-(\bar{\Omega}^+)$  at both RHIC and LHC energies. An increase in the enhancement factor is observed with the increase in strangeness content of the baryons. We also observe that enhancement is higher in Au + Au collisions than in Pb + Pb collisions. Further, we compare the HYDJET++ results with the experimental data and various other simulation models, wherever possible.

DOI: [10.1103/PhysRevC.107.024906](https://doi.org/10.1103/PhysRevC.107.024906)

## I. INTRODUCTION

Our understanding about the physical mechanism of strangeness production in quantum chromodynamic (QCD) medium has evolved significantly through various experimental and theoretical observations since the early 1990s. In earlier days, strangeness enhancement is assumed as sacrosanct signal to detect quark gluon plasma (QGP) phase [1–3]. This QGP phase has several different properties than the low-density hadron gas (HG) phase, e.g., color charges (quarks and gluons) are not confined to a mere hadronic volume but they can move on a larger volume. Strangeness production in early stages of heavy-ion collisions is based on hard partonic interaction processes like flavor creation ( $gg \rightarrow s\bar{s}$ ,  $q\bar{q} \rightarrow s\bar{s}$ ) and/or flavor excitation (e.g.,  $gs \rightarrow gs$ ,  $qs \rightarrow qs$ ) [4]. Afterwards partonic evolution via gluon splitting ( $g \rightarrow s\bar{s}$ ) can further create the strangeness [4]. In the later stage of medium evolution, the most probable way to produce strangeness in HG phase is via associated production channels ( $N + N \rightarrow N + \Lambda + K$ ) [3]. Two main arguments which support the idea of multiplicity enhancement of strange particles in QGP than HG phase are as follows [3]:

First, the  $Q$  value for the partonic reactions by which strange ( $s$ )-antistrange ( $\bar{s}$ ) pair (which can later form strange hadrons at freeze-out) is quite low in QGP than the  $Q$  value of hadronic reactions. The latter phenomenon generates (multi-) strange hadrons directly, when thermal medium created through heavy-ion collisions remains in the hadronic phase during the whole dynamical evolution.

The second argument regards the equilibration time of partonic reactions which is much shorter in comparison to hadronic interactions. To produce (multi-) strange baryons like  $\Omega^-$  in HG, the system has to go with the following reaction chain (or cascade mechanism) [5]: (i)  $\pi^0 + p \rightarrow K^+ + \Lambda$ , (ii)  $\pi^0 + \Lambda \rightarrow K^+ + \Xi^-$ , and (iii)  $\pi^+ + \Xi^- \rightarrow K^+ + \Omega^-$ . Further, the probability of decaying this heavy multistrange hadron into strange hadron is quite large.

These two effects combined together tend to increase the equilibration time for (multi-) strange hadrons up to the order of 100 fm/c. Thus, it would be very difficult to produce (multi-) strange particles (e.g.,  $\Xi$ ,  $\bar{\Xi}$ ,  $\Omega^-$ ,  $\bar{\Omega}^-$ ) profusely in an HG. However, gluon flavor democracy causes equilibration of strangeness very fast in QGP [5]. Consequently, these large number of strangeness can easily fill the phase space during the hadronization according to their equilibrium (chemical) value. Based on the above-mentioned assumptions and observations, practitioners in this field believed that strangeness production can decipher the effect caused by HG or QGP and strangeness enhancement can act as a signal for the detection of QGP. However, in recent decades, it has been found that many other physical processes can affect strange particle

\* arpit.singh@bhu.ac.in

† prashantpmsd@mmt.ac.in

‡ gauri1995devi@gmail.com

§ bksingh@bhu.ac.in

production and alter our understanding about strangeness enhancement [3–5]. One of them is the string-hadronic model, which employs Schwinger mechanism [6] for particle production through fragmenting color fields (strings). In central high-energy heavy-ion collisions, the string density could be so high that the color flux tubes overlap leading to a superposition of the color electric fields. This results in an enhanced production of (multi-) strange hadrons. This mechanism has been employed in the UrQMD model [7] showing an enhancement of (multi-) strange hadrons which grows stronger with the strangeness content resulting in an enhancement of  $\Omega$ 's by a factor of 60 compared to  $p + p$  collisions. Another possible mechanism of strangeness enhancement is the creation of vacuum particles under varying external fields at timescales comparable with the inverse mass of the particles [8]. The dynamics of the production process essentially depends on the form and shape of the field pulse. As Schwinger-like regime of particle creation might not be realized at the typical timescale of QGP formation, i.e.,  $\tau_0 \sim 1$  fm/c, the nonstationary field results in the enhanced production of heavy strange quarks.

A recent suggestion to improve our understanding of strangeness production is that one should treat the QCD medium as a strongly interacting liquid in the temperature range  $T = T_c - 3T_c$  rather than as an ideal gas. This suggestion originates from the experimental observation of elliptic flow ( $v_2$ ) at Relativistic Heavy Ion Collider (RHIC) [9–12]. This modification could alter the equilibration time of strangeness at the partonic stage [13]. Replacing the ideal equation of state with the strongly interacting equation of state manifested by lattice QCD will increase the partonic equilibration time ( $\tau$ ). However, the existence of initial anisotropies which causes plasma instabilities will again decrease the partonic equilibration time [14] and probably neutralizes the effect of change in the equation of state of QCD thermal medium. On the hadronic side, it has been claimed that inclusion of a new multimeson fusion process which generates strange particles can enhance the multiplicity of strange antibaryons [15]. Later, it has been shown that this mechanism is not sufficient for an equilibration during the lifetime of the hadronic state of reaction at and above the highest RHIC energy [16,17]. Another suggestion to explain a quick equilibration within the lifetime of the HG phase is by including the Hagedorn exponential mass spectrum in HG to incorporate the effect of massive hadronic resonances [18,19]. It has also been pointed out that the theoretically probable chiral phase transition can shift the masses of strange mesons toward light mesons which consequently causes a sizable effect on the experimental observables like strange-to-antistrange ratios, etc. [20].

Experimentally, the relative high production of strange hadrons in nucleus-nucleus ( $A + A$ ) collisions with comparison to elementary nucleon-nucleon ( $N + N$ ) collisions is treated as strangeness enhancement. Recent compilation of experimental results by ALICE collaboration has shown a steady increase of strange hadron production with increasing system size, i.e., with the number of participating nucleons ( $N_{\text{part}}$ ) and with increase in the strange quark content [21]. These results are in accordance with the lower-energy experimental results from STAR and NA57 collaborations

[22–24]. However, as discussed above, one should not make any inference regarding production of the QGP phase by observing the relative enhancement in experimental data. The most crucial point in the present experimental situation is whether the enhancement in  $A + A$  collisions is only due to phase-space suppression in the smaller system (e.g.,  $N + N$ ,  $N + A$ , etc.) or whether it is really due to an enhancement in strangeness production from a deconfined QCD medium. Experimental results demonstrated by plotting the variation of mean multiplicity with respect to centrality or  $N_{\text{part}}$  show that the relative increase in strange particle multiplicity is only due to restriction in phase space.  $\Omega$  is exception to these observations since the phase suppression factor becomes almost 1 at  $N_{\text{part}} = 100$  or above at RHIC energy. However, one can see from the RHIC data that a yield of  $\Omega$  still increases and becomes greater than its equilibrium value as calculated in HG and  $\gamma_s \sim 1$  can only accommodate half of the mean multiplicity of the  $\Omega$  baryon. Another important experimental result is that in high-multiplicity  $p - p$  events, strangeness production reaches to the corresponding values observed in Pb-Pb collisions [4]. In  $p$ -Pb collisions at  $\sqrt{s_{NN}} = 5.02$  TeV, the transverse momentum distributions exhibit a hardening as a function of multiplicity which is stronger for heavier strange particles [25].

Since the early 2000s, various simulation models have been put forward in terms of the strangeness production mechanism in heavy-ion collisions at different energies. Some of them are AMPT [26–29], HIJING [30,31], EPOS [32,33], Krakow model [34,35], UrQMD [36,37], VISHNU model [38], etc. HIJING combines perturbative-QCD processes for multiple jet production with low- $p_T$  multistring phenomenology. This model incorporates multiple minijet production, nuclear shadowing, and mechanism for jet interaction in dense matter. AMPT model starts with HIJING initial conditions and then describes particle production via string excitations and breaking (soft) and mini-jet fragmentation (hard) where the excited nucleons fragments independently. Extended AMPT model [29] uses an additional system size-dependent coalescence factor for (multi-) strange hadron production. EPOS and Krakow models are based on a core-corona concept. In EPOS, core-corona splitting is based on the initial energy density rather than participants that undergo multiple collisions. Krakow model introduces nonequilibrium corrections due to viscosity in the transition from a hydrodynamic description to one involving the final-state particles [34,35]. UrQMD is a microscopic transport model which describes phenomenology of hadronic interactions at low and intermediate energies in terms of interactions between known hadrons and their resonances and at higher energies in terms of excitation of color strings and their subsequent fragmentation into hadrons. The VISHNU model uses VISH2 + 1 [39] for QGP fluid expansion and UrQMD [36] for hadron resonance gas evolution. A recent experimental analysis by ALICE collaboration on multistrange particles [21] demonstrated a varying level of agreement of experimental data with different models. In particular, the production of multistrange baryons has not been reproduced by these models. Some of them overestimate and some of them underestimate the yields of multistrange baryons, i.e.,  $\Xi$  and  $\Omega$ . In this article we have

studied the (multi-) strange production in Au + Au collisions at  $\sqrt{s_{NN}} = 200$  GeV and in Pb + Pb collisions at  $\sqrt{s_{NN}} = 2.76$  TeV using the HYDJET ++ model [40]. Basically, we have calculated the transverse momentum distribution ( $p_T$  spectra), particle ratios, and strangeness enhancement factor of (multi-) strange hadrons. The remainder of the paper is organized as follows: Section II provides a brief mechanism of particle production in the HYDJET ++ model. Section III provides the results and discussion under various subsections. In Sec. IV, we summarize our present findings.

## II. HYDJET ++ MODEL

The Monte Carlo HYDJET ++ model generates a heavy-ion event as a superposition of the soft, hydro-type state and the hard state resulting from multiparton fragmentation. Both the states, i.e., soft and hard components, are treated independently. The details on physics model and simulation procedure of HYDJET ++ can be found in the corresponding article [40]. In brief, the hard part of hadron production in HYDJET ++ uses the PYQUEN partonic loss model [41–43] which includes generation of initial parton spectra according to PYTHIA [44], and production vertices are measured at a given impact parameter. After that, the partons are rescattered in the hot and dense zone, and subsequently they hadronize according to the Lund string model [45]. The partonic collisional energy loss due to elastic scattering is calculated in the high momentum transfer limit [46] and the radiative energy loss is treated within BDMS formalism [47,48]. Impact parameter-dependent parametrization obtained within the framework of Glauber-Gribov theory [49] is utilized for incorporating the nuclear shadowing effect on parton distribution functions for hard component. HYDJET ++ employs Pro-Q20 tune [50] of PYTHIA for generation of initial parton spectra where strangeness production is governed by two parameters: PARJ(2) = 0.2 (strangeness suppression) and PARJ(3) = 0.94 (strange diquark suppression).

Soft hadron production is based on a predefined chemical and thermal freezeout hypersurface similar to that of statistical thermal model where particle number density is represented in the form:

$$\rho_i^{\text{eq}}(T, \mu_i) = \frac{g_i}{2\pi^2} \gamma_s^{|n_i^s|} m_i^2 T \sum_{k=1}^{\infty} \frac{(\mp)^{k+1}}{k} \exp\left(\frac{k\mu_i}{T}\right) K_2\left(\frac{km_i}{T}\right), \quad (1)$$

where  $m_i$  and  $g_i = J_i + 1$  are the mass and spin degeneracy factor of hadron  $i$ ,  $\gamma_s$  is strangeness suppression factor,  $n_i^s$  is the number of strange quarks and antiquarks in the  $i$ th hadron, and  $K_2$  is modified Bessel function of the second order. The sign ( $\mp$ ) accounts for the quantum statistics of a boson or a fermion, respectively. Further, the hadron multiplicities are generated using the effective thermal volume approximation and Poisson multiplicity distribution around its mean value. The effective volume is supposed to be proportional to the number of participating nucleons at a given impact parameter of  $A + A$  collision [51,52]. The final-state interaction of the two- and three-body decays of resonances and their branching ratios are taken from the SHARE particle decay table [53]

while calculating the final multiplicity of the produced particle. HYDJET ++ provides an option to choose from different types of freezeout scenarios. One can choose a single freezeout hypersurface for nonstrange and strange particles with no phase suppression for strange particles. The other is a single freezeout hypersurface for nonstrange and strange particles but with a phase suppression factor ( $\gamma_s$ ) for strange production. The functional form of the phase suppression factor ( $\gamma_s$ ) [54] used in HYDJET ++ is

$$\gamma_s = 1 - g \exp\left[-\frac{a}{\mu_B/T}\right], \quad (2)$$

with parameters  $g = 0.396$  and  $a = 1.23$ ;  $\mu_B$  is baryon chemical potential and  $T$  is chemical freezeout temperature. However, Eq. (2) is valid for most central collisions only. Therefore, for present work  $\gamma_s$  is treated as a free parameter. Generally,  $\gamma_s$  is employed as a possible indicator for the deviation of strange quarks from equilibrium in describing the chemical freezeout [55,56]. For noncentral collisions,  $\gamma_s$  shows deviation from unity and for central collisions  $\gamma_s$  approaches unity, suggesting equilibration of strange quarks with the increase in system size [55]. The  $\gamma_s$  values for different centrality intervals are taken from Ref. [55] and kept the same for both RHIC and Large Hadron Collider (LHC) energies. The chemical freezeout temperature,  $T_{\text{ch}}$  (input parameter), is set to 0.1615 GeV and the rest of the parameters are same as in the default version of HYDJET ++.

## III. RESULTS AND DISCUSSIONS

### A. Transverse momentum distribution

HYDJET ++ is one of the very few models which employs soft and hard physics simultaneously to describe particle production in heavy-ion collisions. Therefore, the foremost exercise performed is to observe the contribution of hydro (soft) part and jet (hard) part to the  $p_T$  spectra of (multi-) strange hadrons. Figures 1 and 2 show the  $p_T$  spectra of (multi-) strange hadrons in most central and most peripheral events along with the soft and hard part contributions for Au + Au and Pb + Pb collisions, respectively. It is observed that both the hydro and jet parts contribute to the particle yield from low to intermediate  $p_T$ . However, the contribution from the jet part is relatively small in comparison to the hydro part and it further decreases with an increase in the number of valence strange (anti-) quarks. Moreover, from intermediate to high  $p_T$ , the particle production is dominated solely by the jet part with very little or no contribution from the hydro part. For  $\Xi$  and  $\Omega$ , the bulk of the yield is from hydro production of hadrons for both Au + Au and Pb + Pb collisions.

Having the essence of hydro and jet productions for (multi-) strange hadron, the  $p_T$  spectra obtained from the HYDJET ++ model for  $K$ ,  $K_s^0$ ,  $\Lambda$ ,  $\Xi$ , and  $\Omega$  and corresponding antiparticles are presented and compared with the experimental data in different centrality intervals for Au + Au and Pb + Pb collisions. For better visualization,  $p_T$  spectra of the experiment and the model are divided by factors of 10 from central to peripheral collisions. The normalization factors are also mentioned in the legend of corresponding figures.

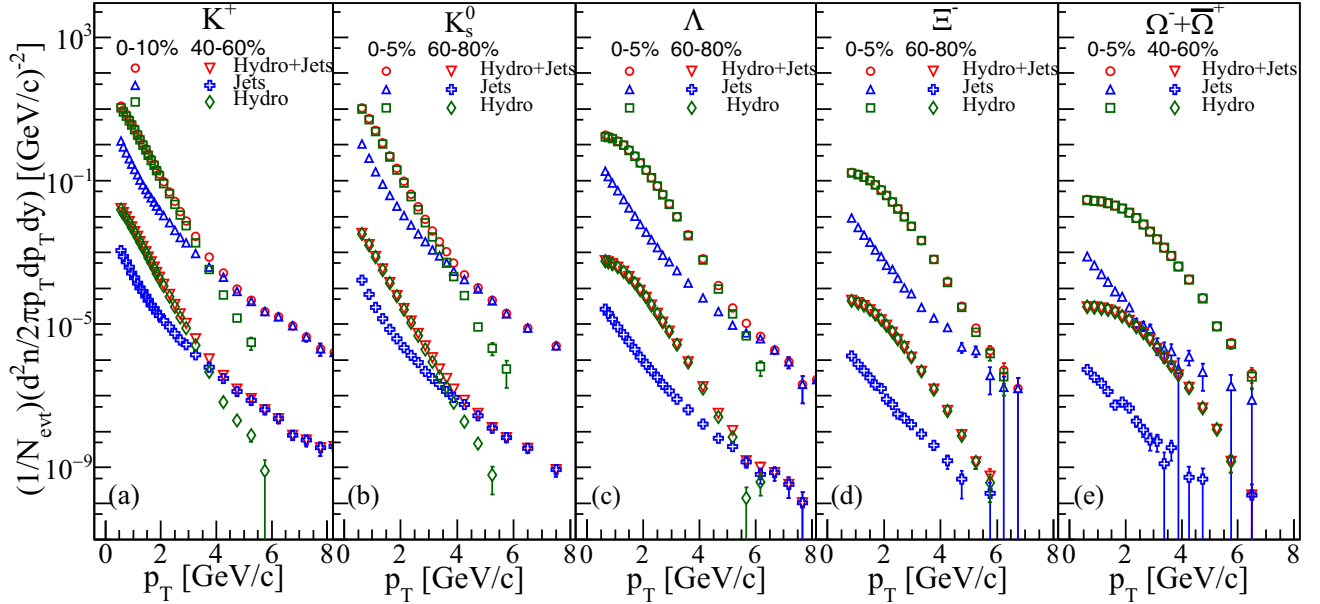


FIG. 1. Transverse momentum ( $p_T$ ) spectra of (a)  $K^+$ , (b)  $K_s^0$ , (c)  $\Lambda$ , (d)  $\Xi^-$ , and (e)  $\Omega^- + \bar{\Omega}^+$  in Au + Au collisions at  $\sqrt{s_{NN}} = 200$  GeV. The results for most central and most peripheral centrality interval are shown along with the contribution from jet part and hydro part.

One of the key points to mention regarding (multi-) strange hadron production in the present calculation is the contribution of weak decays. The weak decay channels and their branching ratios considered for (multi-) strange hadrons in the model are as follows:

For  $\Lambda$ :  $\Lambda \rightarrow p + \pi^-$  (64%),  $\Lambda \rightarrow \Delta + \pi^0$  (36%).

For  $\Xi$ :  $\Xi^- \rightarrow \Lambda + \pi^-$  (100%).

For  $\Omega$ :  $\Omega^- \rightarrow \Lambda + K^-$  (68%),  $\Omega^- \rightarrow \Xi^0 + \pi^-$  (24%),  
 $\Omega^- \rightarrow \Xi^- + \pi^0$  (8%).

For  $K_s^0$ :  $K_s^0 \rightarrow \pi^+ + \pi^-$  (68.6%),  $K_s^0 \rightarrow \pi^0 + \pi^0$  (31.4%),

and their charge conjugate for antiparticle decays. However, strange hadrons in experimental analysis are measured through reconstruction of weak decay topology in channels:  $\Lambda \rightarrow p + \pi^-$  (64%),  $\Xi^- \rightarrow \Lambda + \pi^-$  (99.9%),  $\Omega^- \rightarrow \Lambda + K^-$  (67.8%), and  $K_s^0 \rightarrow \pi^+ + \pi^-$  (69.2%) and their charge conjugate for antiparticle decays. Further, the  $\Lambda$  spectra is corrected for the feed-down contribution from the weak de-

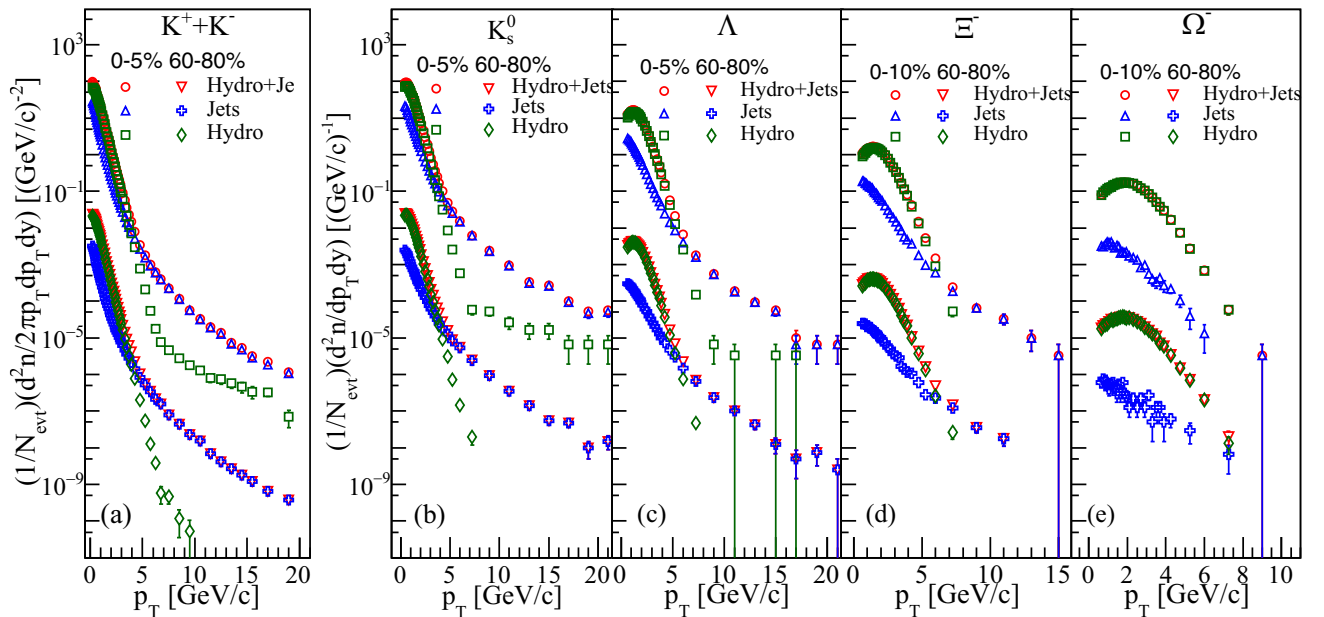


FIG. 2. Transverse momentum ( $p_T$ ) spectra of (a)  $K^+ + K^-$ , (b)  $K_s^0$ , (c)  $\Lambda$ , (d)  $\Xi^-$ , and (e)  $\Omega^-$  in Pb + Pb collisions at  $\sqrt{s_{NN}} = 2.76$  TeV for most central and most peripheral centrality intervals. Contribution from jet part and hydro part is also shown.



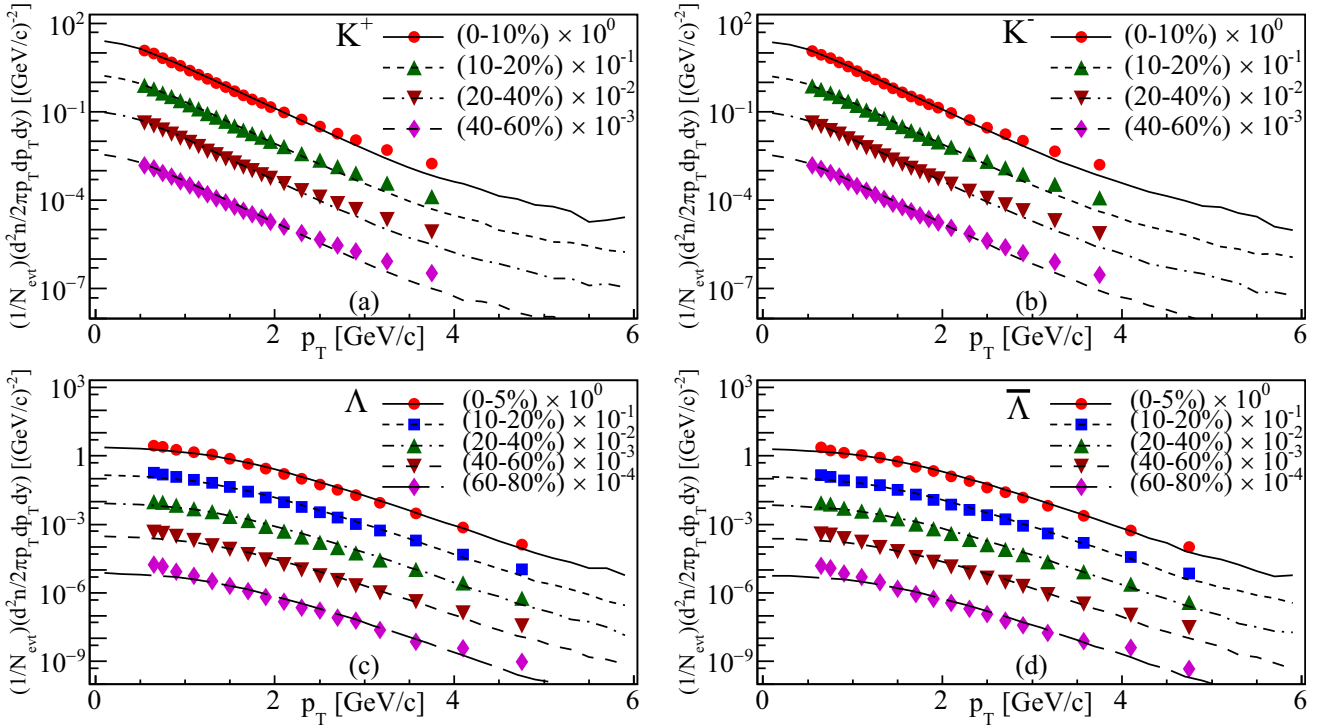


FIG. 3. Transverse momentum ( $p_T$ ) spectra of (a)  $K^+$ , (b)  $K^-$ , (c)  $\Lambda$ , and (d)  $\bar{\Lambda}$  for different centrality intervals in Au + Au collisions at  $\sqrt{s_{NN}} = 200$  GeV. Different markers show PHENIX [57] and STAR [55] Collaboration data, and lines represent the HYDJET++ model result.

cays of  $\Xi^-$  and  $\Xi^0$  at LHC energy. Therefore, the HYDJET++ calculations are expected to overpredict (multi-) strange particle spectra at both RHIC and LHC energies. Also, the contribution of weak decay of resonances taken from the SHARE particle decay table further boosts the strange hadron spectra in comparison with experimental data.

Figures 3 and 4 show the  $p_T$  spectra of  $K^+$ ,  $K^-$ ,  $\Lambda$ ,  $\Xi^-$ ,  $\Xi^+$ ,  $K_s^0$ , and  $\Omega^- + \bar{\Omega}^+$  obtained from the HYDJET++ model for Au + Au collisions at  $\sqrt{s_{NN}} = 200$  GeV in different centrality intervals. The model results are compared with the measurements performed by the PHENIX Collaboration [57] and STAR Collaboration [55]. Similarly, Figs. 6 and 7 show the  $p_T$  spectra of  $K^+ + K^-$ ,  $\Lambda$ ,  $K_s^0$ ,  $\Xi^-$ ,  $\Xi^+$ ,  $\Omega^-$ , and  $\bar{\Omega}^+$  obtained from the model along with the experimental results from ALICE Collaboration [21,59,60] for Pb + Pb collisions at  $\sqrt{s_{NN}} = 2.76$  TeV. Figures 5 and 8 show the model-to-data ratios of measured  $p_T$  spectra of strange hadrons for Au + Au and Pb + Pb collisions, respectively. It can be seen that the model-to-data ratio of kaons ( $K$  and  $K_s^0$ ) are suppressed by a factor of 2 in the  $p_T \approx 3\text{--}5$  GeV/c interval where jet contribution start to dominate the particle production (as evident from Figs. 1 and 2). This might be explained in terms of the strangeness suppression factor ( $\gamma_s$ ). HYDJET++ uses Pro-Q20 tune of Pythia with  $\gamma_s$ , i.e., factor PARJ(2), fixed to 0.2. The authors in Ref. [61,62] introduced a reduction mechanism for strange quark suppression in Pythia assuming the effective string tension increases with increase in reaction energy. The reduction mechanism improves strange quark

production from Pythia. However, at higher  $p_T$ , the agreement between the model result and experimental data is improved for kaons [see Figs. 5(c) and 8(c)]. It indicates that the hard scattering processes provide a good description of strangeness production at higher  $p_T$ . It can also be observed that the model-to-data ratio of  $\Lambda$  and  $\Xi$  is increased by a factor of 1.5 in  $p_T \approx 2\text{--}4$  GeV/c toward peripheral collisions. It may be due to the consideration of 100% production of strange baryons through weak decay channels as described earlier while in experimental results only most prominent decay channels are used for strange baryon reconstruction. Moreover, the model-to-data ratio of pure baryonic strange state  $\Omega$  is increased by a factor of 3 in Au + Au collisions and by a factor of 2 in Pb + Pb collisions at intermediate  $p_T$  region. It indicates that strange quark thermalization might not be achieved by the model for pure baryonic strange state  $\Omega$  and toward peripheral collisions for  $\Lambda$  and  $\Xi$  baryons. Therefore, the value of  $\gamma_s$  used in present analysis taken from Ref. [55] does not properly thermalize the medium especially for  $\Omega$  baryon. Further, the author in Ref. [63] introduced an additional diquark and strange diquark suppression factor along with  $\gamma_s$  in thermodynamical model similar to quark jet fragmentation model to improve the strange particle production. It will be interesting to incorporate these additional parameters in the model and observe their effect on strange hadron production. We leave this exercise for our future work where we will study the production of pure strange states,  $\phi$  and  $\Omega$ , by retuning the strangeness suppression factor ( $\gamma_s$ ).

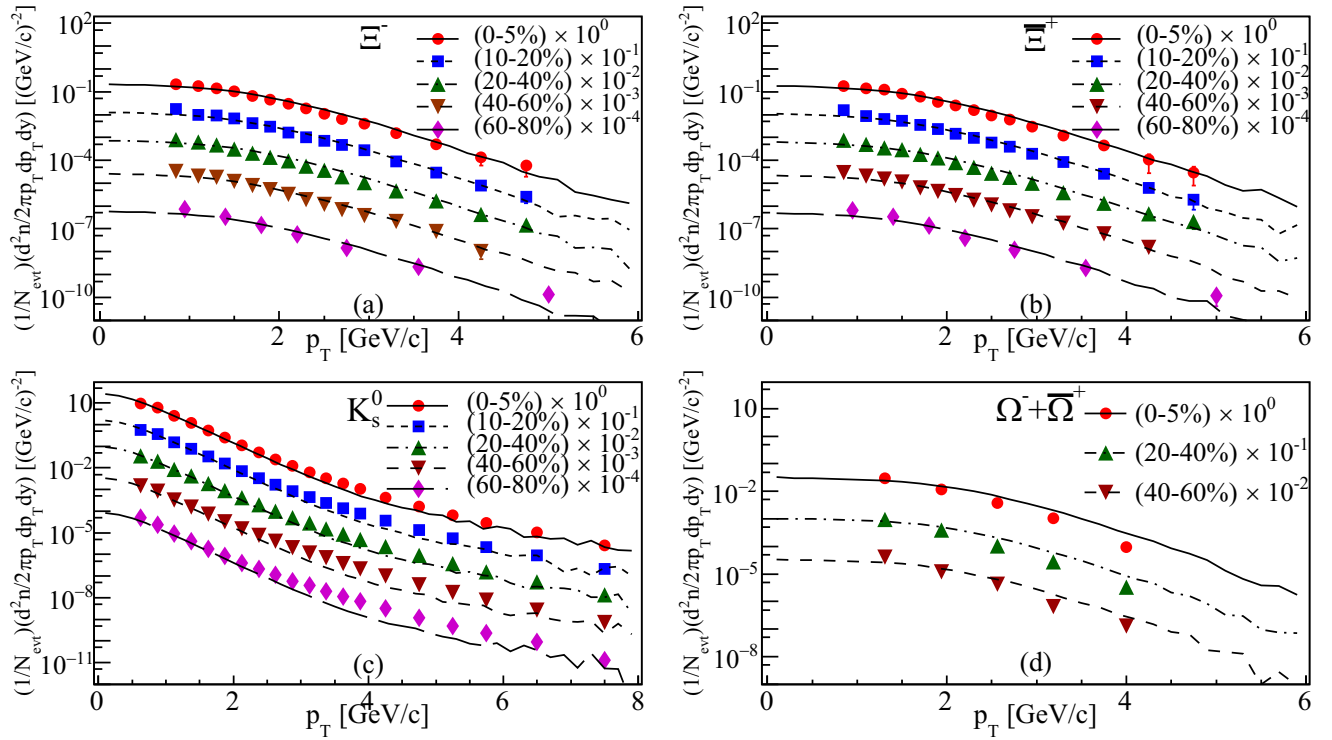


FIG. 4. Transverse momentum ( $p_T$ ) spectra of (a)  $\Xi^-$ , (b)  $\Xi^+$ , (c)  $K_s^0$ , and (d)  $\Omega^- + \bar{\Omega}^+$  for different centrality intervals in Au + Au collisions at  $\sqrt{s_{NN}} = 200$  GeV. Different markers show STAR Collaboration data [55,58], and lines represent the HYDJET++ result.

In Fig. 9, a comparison of HYDJET++ model  $p_T$  spectra is performed with VISHNU [38,64], AMPT [65], and EPOS [21] model results. The model results are also

compared with the experimental data. Results for Au + Au collisions at  $\sqrt{s_{NN}} = 200$  GeV and Pb + Pb collisions at  $\sqrt{s_{NN}} = 2.76$  TeV are presented in Figs. 9(a) and 9(b), re-

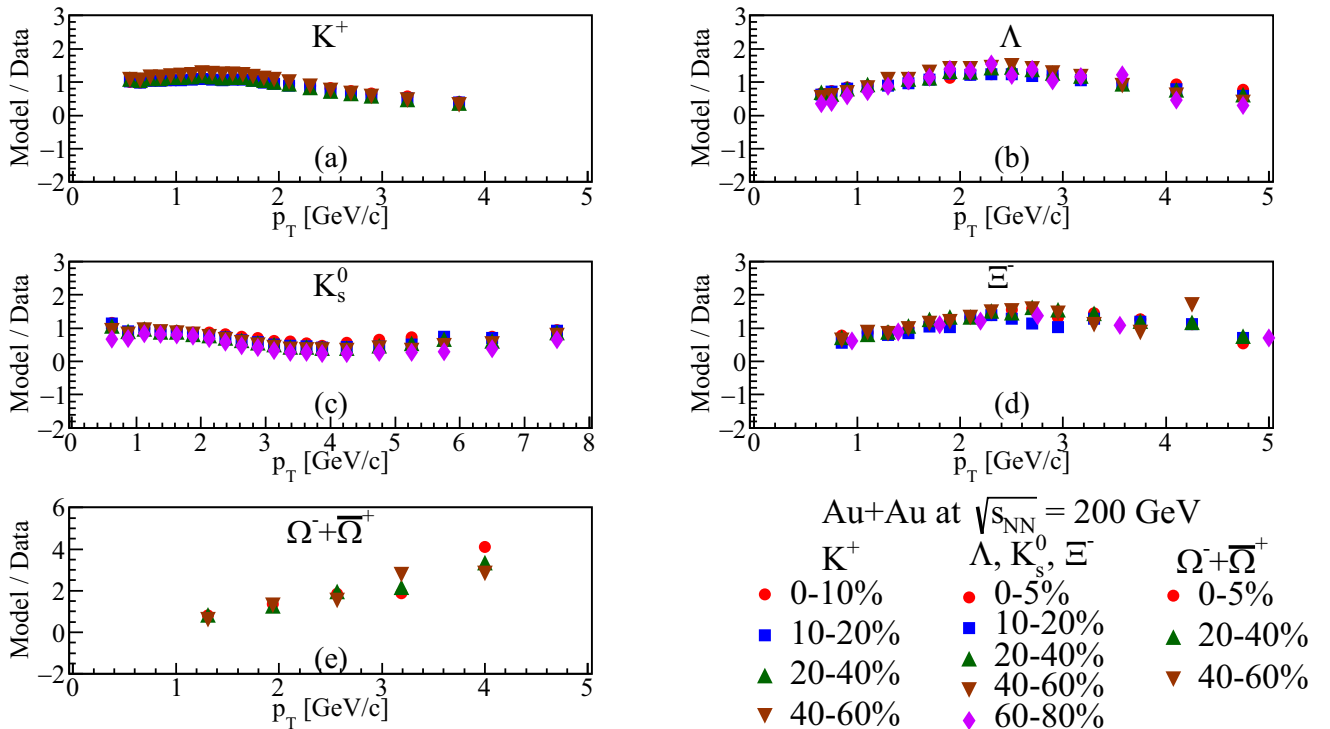


FIG. 5. Model-to-data ratio of different strange particles in Au + Au collisions.

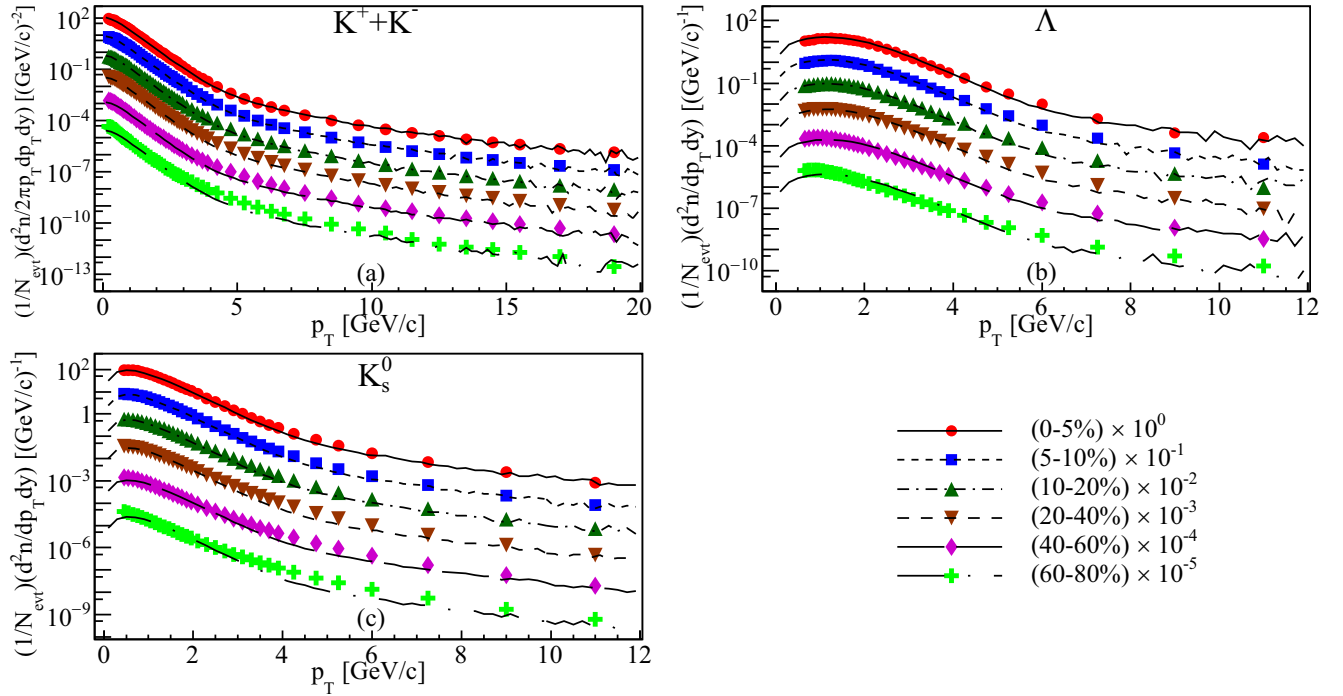


FIG. 6. Transverse momentum ( $p_T$ ) spectra of (a)  $K^+ + K^-$ , (b)  $\Lambda$ , and (c)  $K_s^0$  for different centrality intervals in Pb + Pb collisions at  $\sqrt{s_{NN}} = 2.76$  TeV. Different markers show ALICE Collaboration data [59,60], and lines represent the HYDJET++ result.

spectively. Only most central and most peripheral events are shown. AMPT results are shown for  $\Lambda$  and  $\Xi^-$  in Au + Au collisions. For Pb + Pb collisions, AMPT result for  $\Omega^-$  in 0–5% centrality interval is also presented. The invariant spec-

tra for VISHNU and AMPT is only up to  $p_T \approx 2.8$  GeV/c in Au + Au collisions and Pb + Pb collisions. EPOS data correspond to the average of particle and antiparticle for  $\Xi$  and  $\Omega$ .

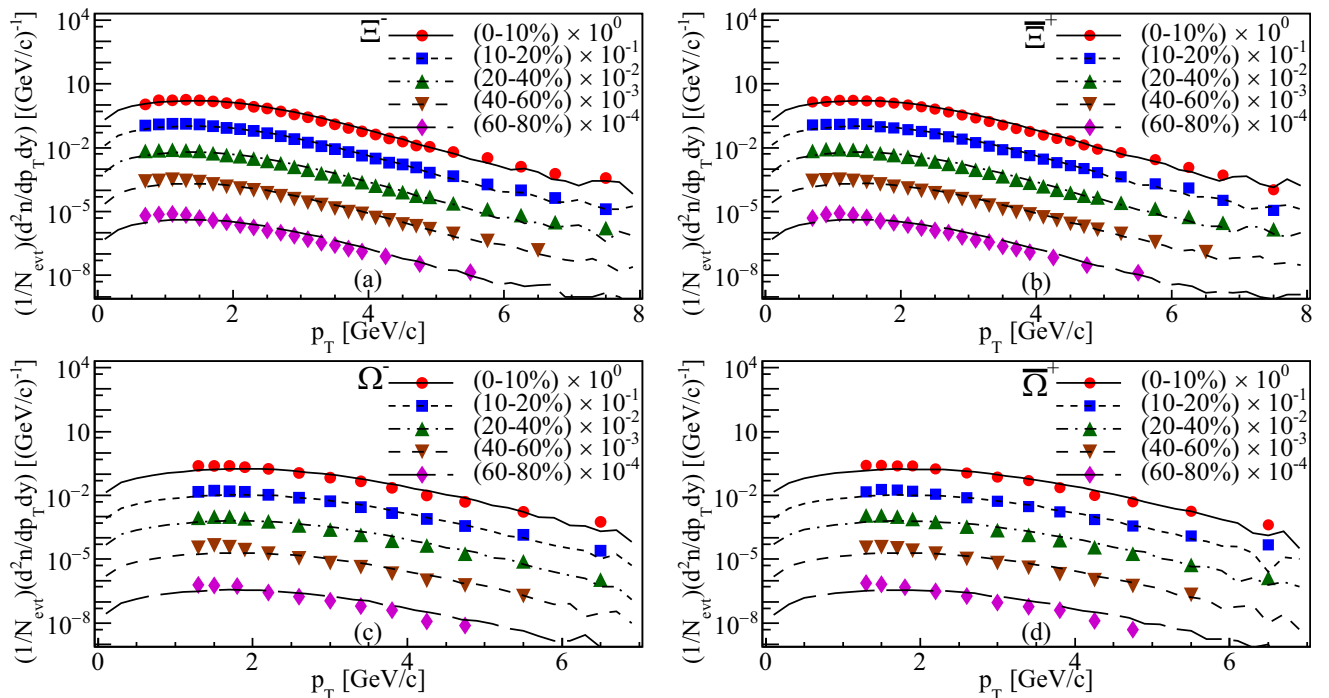


FIG. 7. Transverse momentum ( $p_T$ ) spectra of (a)  $\Xi^-$ , (b)  $\Xi^+$ , (c)  $\Omega^-$ , and (d)  $\Omega^+$  for different centrality intervals in Pb + Pb collisions at  $\sqrt{s_{NN}} = 2.76$  TeV. Different markers show ALICE Collaboration data [21], and lines represent HYDJET++ result.

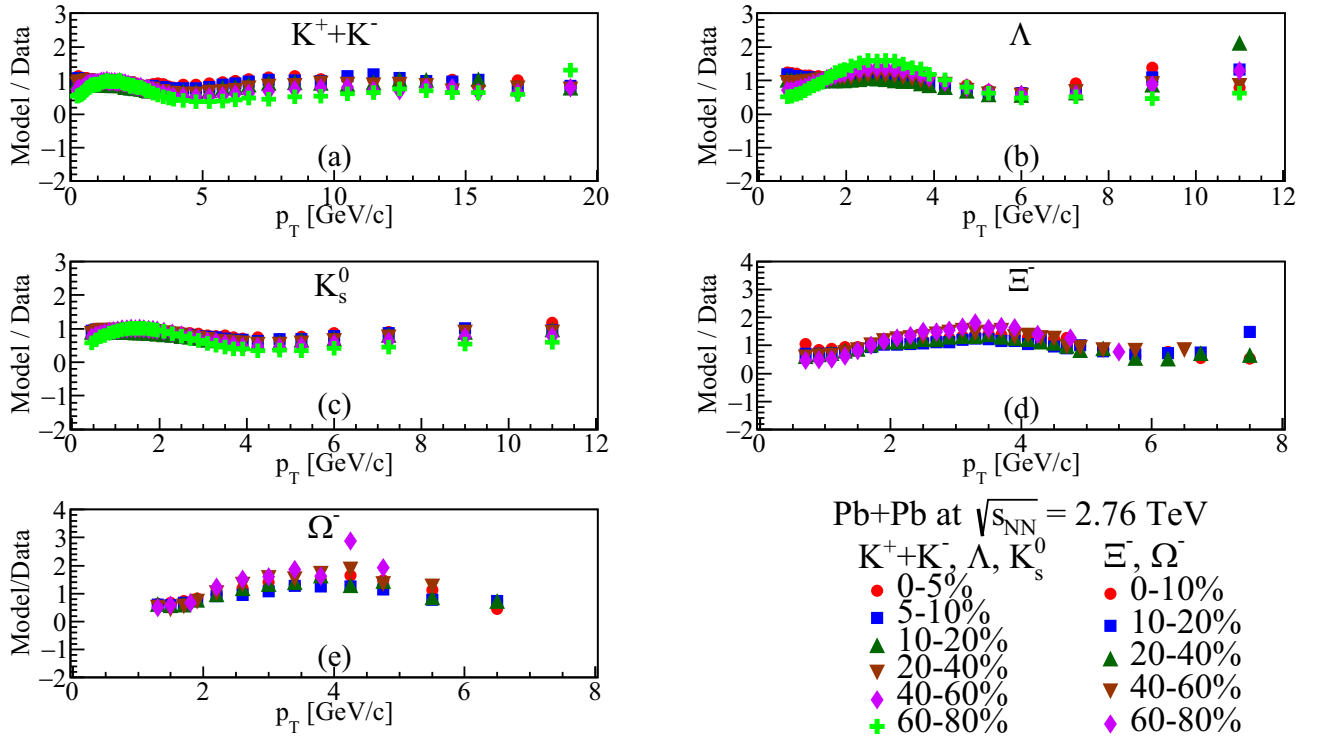
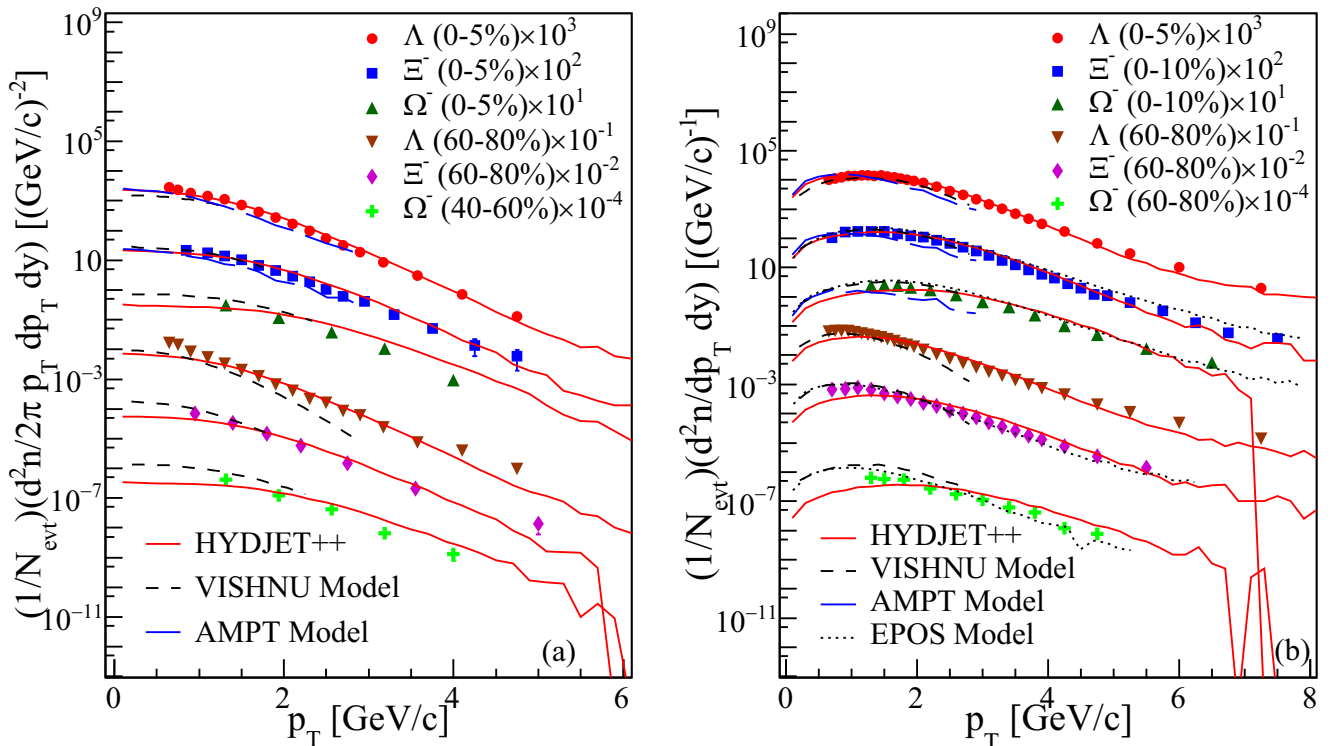


FIG. 8. Model-to-data ratio of different strange particles in Pb + Pb collisions.

FIG. 9. Comparison of HYDJET ++, VISHNU [38,64], AMPT [65], and EPOS [21] model transverse momentum spectra for different strange particles in (a) Au + Au collisions at  $\sqrt{s_{NN}} = 200$  GeV and (b) Pb + Pb collisions at  $\sqrt{s_{NN}} = 2.76$  TeV. Different markers show STAR [55] and ALICE [21,60] experiment data.



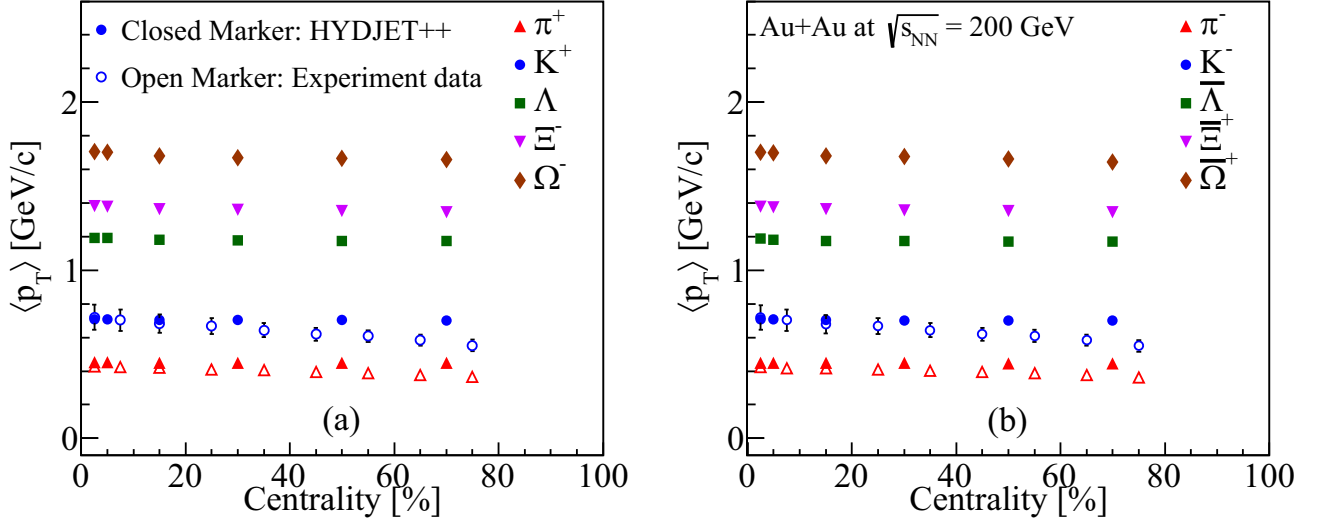


FIG. 10. Mean  $p_T$  as a function of centrality in Au + Au collisions. Solid markers represent HYDJET++ results while open markers represent STAR experiment data [66].

From Fig. 9(a), it is observed that HYDJET++ provides a good description of experimental data for  $\Lambda$  and  $\Xi^-$  in both central and peripheral collisions. It overestimates  $\Omega^-$  spectra toward high  $p_T$ . VISHNU model reproduces the  $p_T$  spectra of  $\Xi^-$  in central and peripheral collisions. It underestimates  $\Lambda$  spectra due to production of  $\Lambda$  from strong resonance decays from UrQMD part of VISHNU [64]. AMPT model also underestimates strange baryon  $p_T$  spectra because strangeness production and annihilation processes are not included in the model [65]. In Fig. 9(b), HYDJET++ and EPOS model results are in good agreement with the experimental data of (multi-) strange baryons in central collisions. AMPT and VISHNU models exhibit similar behavior as observed in the case of Au + Au collisions. In peripheral collisions, the quality of agreement with the experimental data deteriorates for  $\Omega^-$  in both the HYDJET++ and EPOS models. VISHNU model overestimates the  $p_T$  spectra of  $\Omega^-$  in peripheral collisions indicating that chemical equilibrium is not achieved for  $\Omega$  baryons in smaller systems created toward peripheral collisions [38]. Moreover, only the EPOS and HYDJET++ models convincingly reproduce the experimental data for full  $p_T$  range.

Figures 10 and 11 show the variation of mean  $p_T$  of various hadrons as a function of centrality for Au + Au and Pb + Pb collisions, respectively. The results from STAR [66] and ALICE [67] collaborations for pions and kaons are also presented for comparison. In contrast to experimental data, where mean  $p_T$  shows dependence on centrality toward peripheral collisions for pions and kaons, the model results are independent of centrality for all the hadrons. In central collisions, mean  $p_T$  of pions and kaons matches with the experimental data for both the collision systems. However, toward peripheral collisions the model overpredicts the experimental mean  $p_T$  data for  $\pi$  and  $K$ . This indicates that thermal equilibrium might not be achieved for smaller system formed toward peripheral collisions.

## B. Particle ratios

Being independent of most of the systematic uncertainties such as volume fluctuations, measurement of particle ratios helps in characterizing the environment created in heavy-ion collisions by providing information on the net baryon density or baryon chemical potential achieved. In this section, a systematic study of antiparticle-to-particle ratio and ratios of (multi-) strange hadrons with respect to pions, kaons, and  $K_s^0$  has been presented.

Figures 12 and 13 show the antiparticle-to-particle ratio as a function of transverse momentum ( $p_T$ ) in Au + Au collisions at  $\sqrt{s_{NN}} = 200$  GeV and Pb + Pb collisions at  $\sqrt{s_{NN}} = 2.76$  TeV, respectively. The ratios of  $\pi^-/\pi^+$ ,  $K^-/K^+$ ,  $\bar{\Lambda}/\Lambda$ ,  $\bar{\Xi}^+/\Xi^-$ , and  $\bar{\Omega}^+/\Omega^-$  obtained from the HYDJET++ model for 0–5% and 40–60% centrality intervals are presented. It is observed that all the ratios are independent of  $p_T$  and centrality for both Au + Au and Pb + Pb collisions. However, the antiparticle-to-particle ratio is expected to vary as a function of  $p_T$  at high  $p_T$  based on the arguments of parton distribution functions, fragmentation functions, and isospin conservation [68]. In Au + Au collisions, the  $\pi^-/\pi^+$  ratio is approximately unity and  $K^-/K^+$  is slightly lower than unity. This observation is in accordance with the measurements of the PHENIX Collaboration [57]. Further, a mass hierarchy in antibaryon-to-baryon ratios of  $\bar{\Lambda}/\Lambda$ ,  $\bar{\Xi}^+/\Xi^-$ , and  $\bar{\Omega}^+/\Omega^-$  are being observed suggesting a small difference between antibaryon and baryon content for heavy strange baryons. In Pb + Pb collisions, all the antiparticle-to-particle ratios are close to unity due to vanishing baryon chemical potential at the LHC energy regime.

Figure 14 shows  $p_T$  differential ratios of (multi-) strange hadrons with respect to pions and kaons in Au + Au collisions at  $\sqrt{s_{NN}} = 200$  GeV for 0–5% and 40–60% centrality intervals obtained from the model. It can be seen that all the particle ratios with respect to  $\pi$  and  $K$  shows strong  $p_T$  dependence except for the  $K_s^0/K$  ratio, which is independent

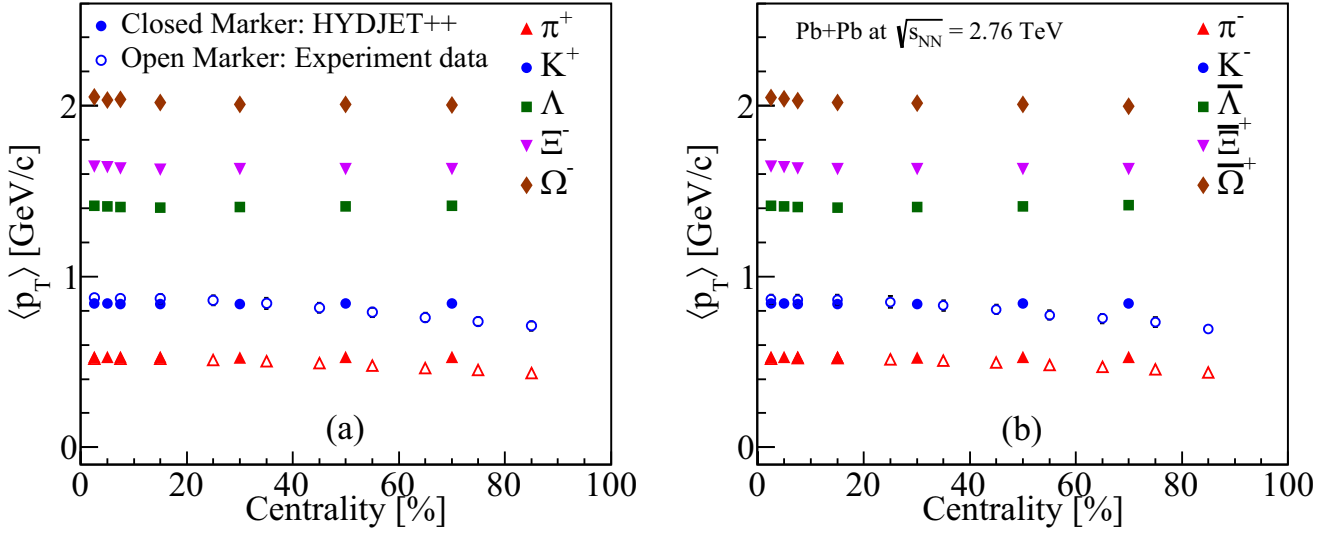


FIG. 11. Mean  $p_T$  as a function of centrality in Pb + Pb collisions. Solid markers represent HYDJET++ results while open markers represent ALICE experiment data [67].

of  $p_T$ .  $K$  and  $K_s^0$  mesons having single valence strange quark and nearly the same mass are produced in the same quantity throughout the  $p_T$  space. At low  $p_T$ , a gradual increase in particle ratios of  $\Lambda$ ,  $\Xi$ , and  $\Omega$  with respect to mesons ( $\pi$  and  $K$ ) are observed. It may be because of the high probability of light meson formation rather than heavy strange baryons at low  $p_T$ . However, the  $K/\pi$  ratio shows a more rapid increase than baryon-to- $\pi$  ratios at low  $p_T$ . It may be due to the high probability of  $K$  meson formation via a combination of strange ( $s$ ) quark and an up ( $u$ ) or down ( $d$ ) quark rather than strange baryon formation by combination of three quarks. Moving toward intermediate  $p_T$ , the particle ratios with respect to  $\pi$  and  $K$  mesons increase because the particle momentum becomes comparable or more than the mass of

strange quarks, which considerably increases the probability of strange baryon formation. The increase in the baryon-to-meson ratio at intermediate  $p_T$  may also be due to the slightly higher momentum of thermal partons produced in the (semi-) hard process, which favors the formation of baryons over mesons because of higher quark content of the former ones [3,69]. At high  $p_T$ , the fragmentation function of jets are suppressed for strange particles compared to nonstrange particles [70]. This results in producing a large number of  $u$  and  $d$  quarks compared to  $s$  quarks and hence the particle ratios with respect to mesons starts to decrease at high  $p_T$ .

The model results for the  $K/\pi$  ratio are compared with the PHENIX Collaboration data [57] of the  $K^+/\pi^+$  ratio for 0–10% and 40–60% centrality intervals in Figs. 14(a) and

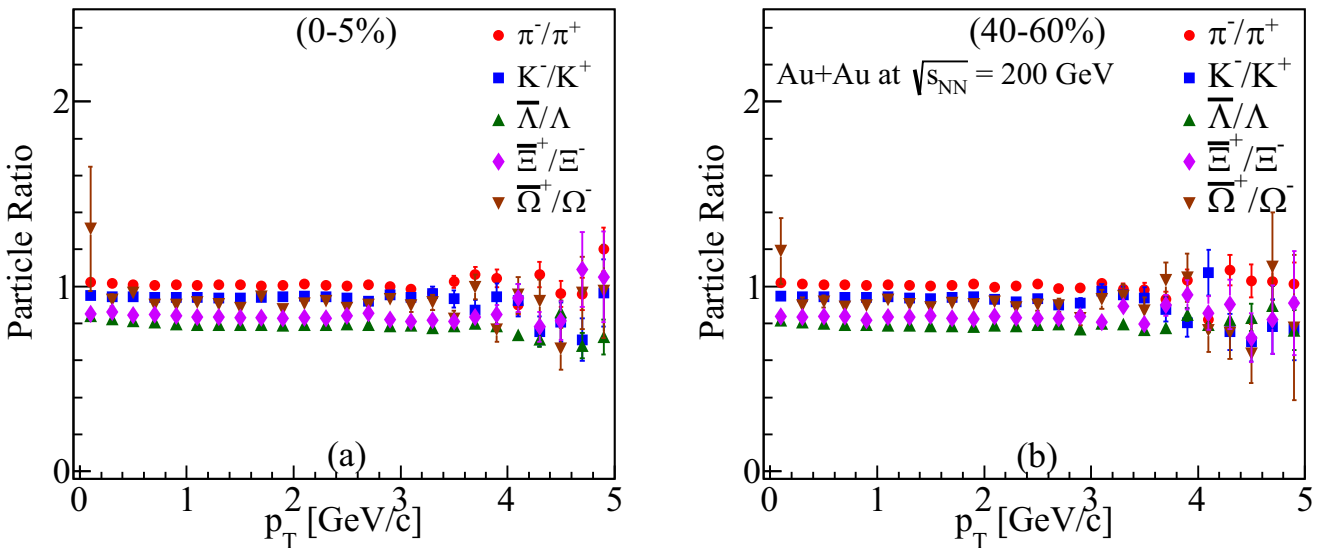


FIG. 12. Antiparticle-to-particle ratio of various strange particle species in (a) 0–5% centrality interval and (b) 40–60% centrality interval for Au + Au collisions at  $\sqrt{s_{NN}} = 200$  GeV.

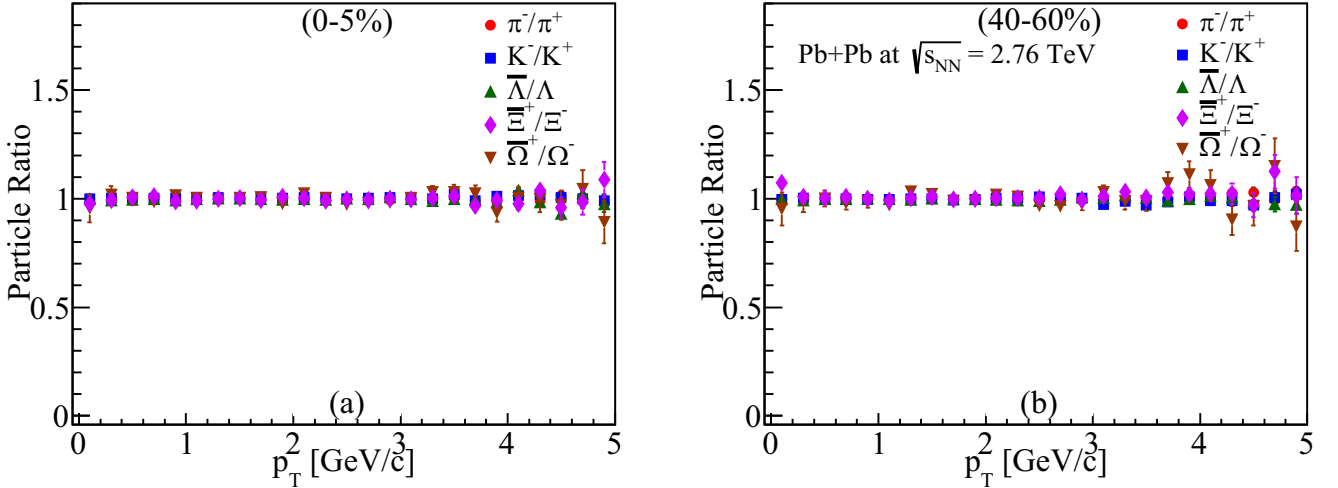


FIG. 13. Antiparticle-to-particle ratio of different strange particle species in (a) 0–5% centrality interval and (b) 40–60% centrality interval for Pb + Pb collisions at  $\sqrt{s_{NN}} = 2.76$  TeV.

14(b), respectively. It can be observed that the model result for the 0–5% and 40–60% centrality intervals reproduces the experimental data of the  $K/\pi$  ratio for the 0–10% and 40–60% centrality intervals up to  $p_T \approx 2$  GeV/c. For  $p_T > 2$  GeV/c, the model underestimates the experimental data because of the lack of kaon yield in this  $p_T$  region. It can be seen from Fig. 3 that the model produces a softer kaon  $p_T$  spectra for  $p_T > 2$  compared to the experimental data. For the strange baryon- ( $\Lambda$ ,  $\Xi$ , and  $\Omega$ ) to-meson ratios, it can be observed that

the peak at intermediate  $p_T$  decreases and moves toward high  $p_T$  with an increase in valence (anti-) strange quark content and mass of strange baryons. The shift of the peak toward high  $p_T$  is attributed to the radial flow generated during the hydrodynamical evolution of the system, which would have pushed heavier baryons to higher momentum. It can be seen from Figs. 10 and 11 that heavier particles have large mean  $p_T$  compared to lighter ones. Moreover, the peak of the  $\Lambda/\pi$  ratio is more than 1 at intermediate  $p_T$ , indicating higher  $\Lambda$  baryon

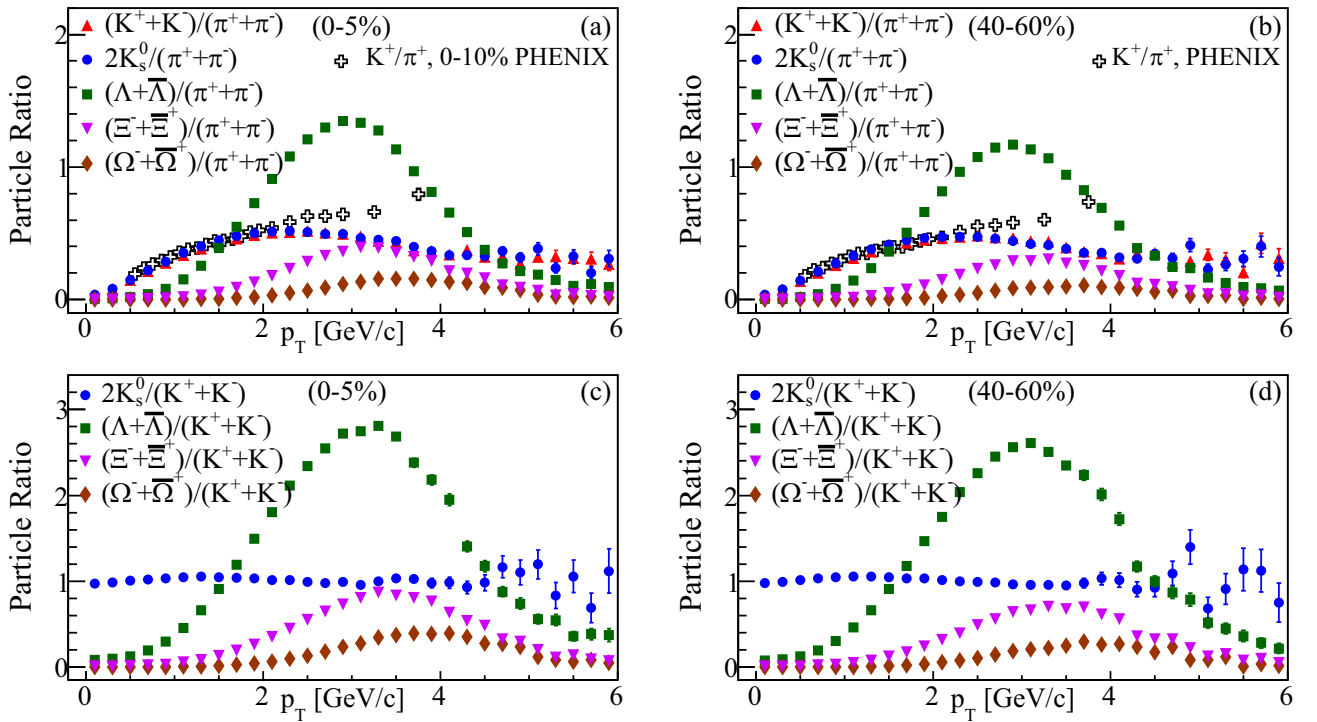


FIG. 14. Ratio of strange hadrons with respect to  $\pi^+ + \pi^-$  for Au + Au collisions in (a) 0–5% centrality interval and (b) 40–60% centrality interval. Similarly, the ratio of strange hadrons with respect to  $K^+ + K^-$  as a function of  $p_T$  is shown in (c) and (d). PHENIX experiment data [57] are also shown.

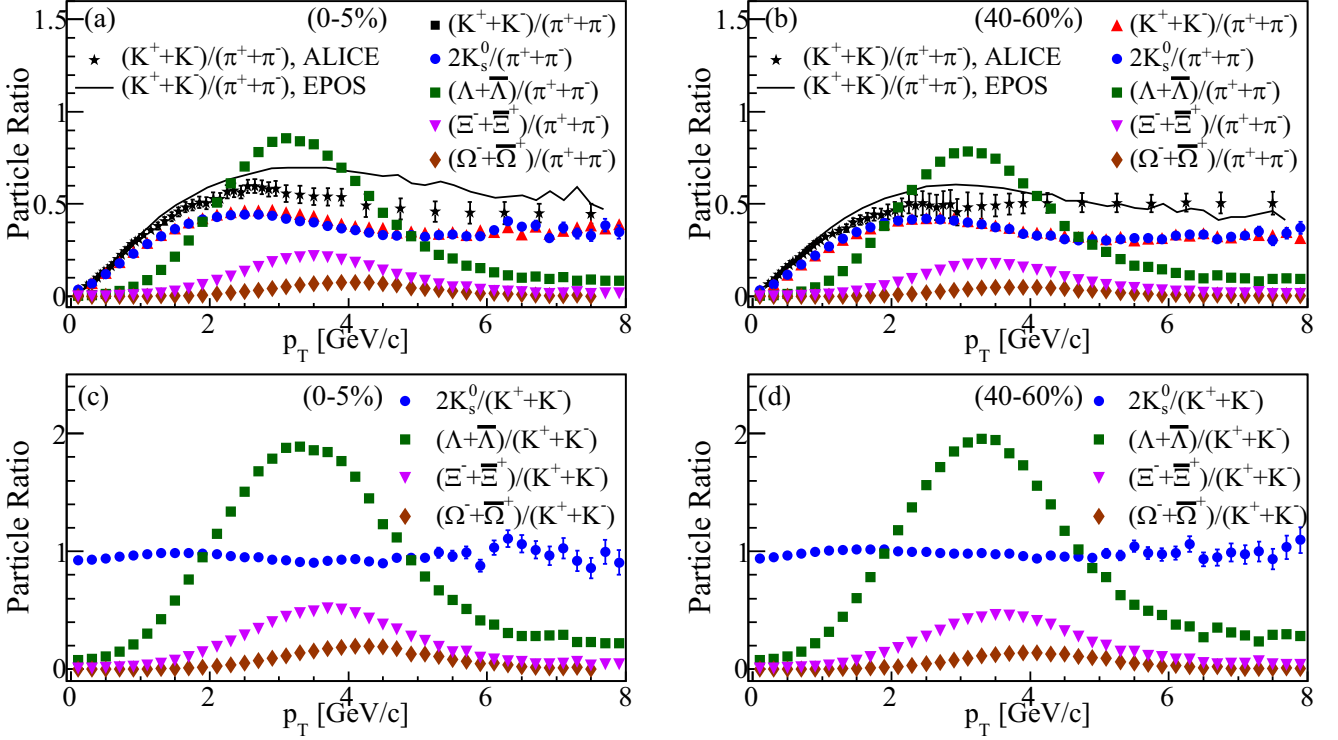


FIG. 15. Ratio of strange hadrons with respect to  $\pi^+ + \pi^-$  for Pb + Pb collisions in (a) 0–5% centrality interval and (b) 40–60% centrality interval. Similarly, the ratio of strange hadrons with respect to  $K^+ + K^-$  as a function of  $p_T$  is shown in (c) and (d). ALICE experiment data [59] are also shown.

production compared to  $\pi$  mesons. The particle ratios with respect to kaons ( $K^+ + K^-$ ) show around a twofold increase in magnitude compared to pion ratios because of the decreased production of  $K$  mesons compared to  $\pi$  mesons due to the heavier mass of the former one.

Figure 15 shows (multi-) strange hadron ratios with respect to pions and kaons as a function of  $p_T$  for Pb + Pb collisions at  $\sqrt{s_{NN}} = 2.76$  TeV in the 0–5% and 40–60% centrality intervals. The variation of particle ratios in Pb + Pb are similar to that observed in Au + Au collisions. However, the magnitude of baryon to meson enhancement is smaller compared to Au + Au collisions. The reason may be the vanishing baryon chemical potential at LHC energies which reduces baryon yield in comparison with mesons at LHC energies. Comparing the model results of the  $K/\pi$  ratio with the ALICE Collaboration [59] data in both the centralities, it can be seen that the model correctly reproduces the shape of the experimental data but it underpredicts the data in the 0–5% centrality interval. However, the  $K/\pi$  ratio obtained by the model approximately matches with the experimental data in 40–60% centrality interval for  $p_T$  up to 3 GeV/c. For  $p_T > 3$  GeV/c, the model underpredicts the experimental data as also observed in the case of Au + Au collisions. It can also be seen that the EPOS model [59] reproduces the kaon-to-pion ratio from central to peripheral collisions but it overpredicts the magnitude of the kaon-to-pion peak.

Figures 16 and 17 show the ratios of  $\Lambda$ ,  $\Xi$ , and  $\Omega$  to  $K_s^0$  as a function of  $p_T$  in the 0–5% and 40–60% centrality intervals for Au + Au collisions at  $\sqrt{s_{NN}} = 200$  GeV and

Pb + Pb collisions at  $\sqrt{s_{NN}} = 2.76$  TeV, respectively. It can be seen that the shape and scale of strange baryon to  $K_s^0$  is similar to the strange baryon-to-kaon ratios. The model results of the  $\Lambda/K_s^0$  ratio are compared with the results of the STAR [58] and the ALICE Collaboration [60] for Au + Au and Pb + Pb collisions in the 0–5% and 40–60% centrality intervals. It can be seen that the  $\Lambda/K_s^0$  ratio is reproduced well by the model at low  $p_T$  and high  $p_T$  for both Au + Au and Pb + Pb collisions. However, at intermediate  $p_T$ , the model overestimates the experimental data at both the energies and centralities. The reason may be the lack of  $K_s^0$  yield in this region that appears quite large in linear scale. It can also be seen from Figs. 4(c) and 6(c) that  $p_T$  spectra of  $K_s^0$  is softer in the model as compared with experimental data. The  $\Lambda/K_s^0$  ratio obtained by AMPT model in Xe-Xe collisions at  $\sqrt{s_{NN}} = 5.44$  TeV [71] shows similar behavior at low and intermediate  $p_T$ , where the AMPT-SM version overpredicts the ALICE data at intermediate  $p_T$ . However, it is shown that the AMPT-Default version provides a better description of the data than AMPT-SM. The authors argue that the coalescence mechanism involved in AMPT-SM affects the particle production at intermediate  $p_T$ . The EPOS model results for the  $\Lambda/K_s^0$  ratio [69] describe the trend observed in the experimental data. It can also be observed in the experimental data of baryon-to-meson ratios [58,60] that the peak moves to higher  $p_T$  going from peripheral to central collisions. This trend is also observed in EPOS model calculations. However, this trend is not observed in HYDJET++ calculations. It may be seen from Figs. 10 and 11 that mean  $p_T$  is independent of centrality

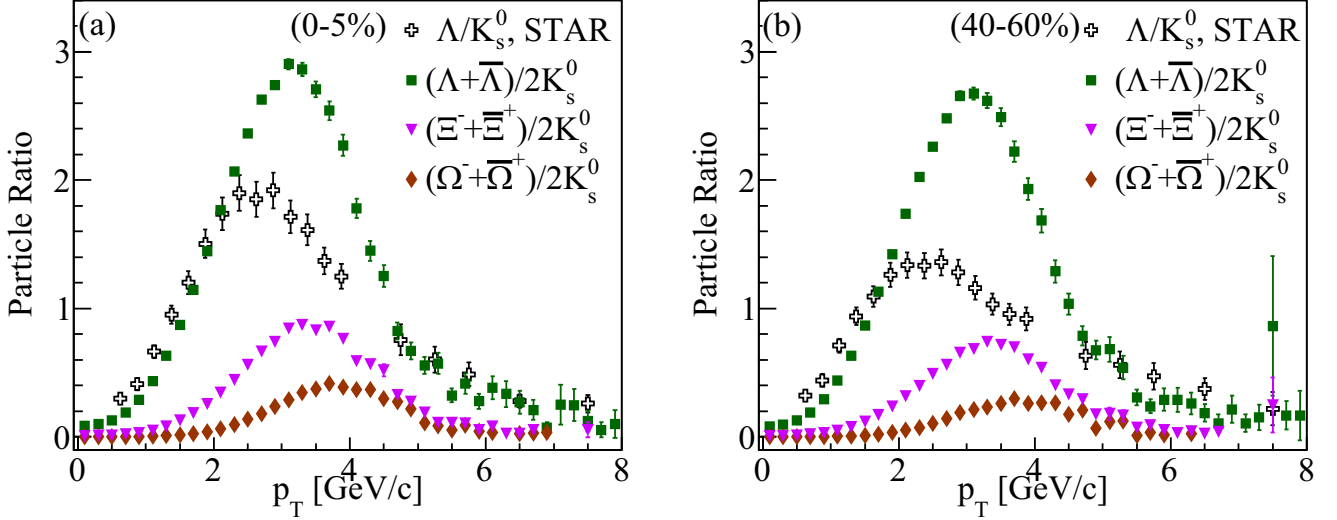


FIG. 16. Strange hadron to  $K_s^0$  ratio as a function of  $p_T$  for centrality interval (a) 0–5% and (b) 40–60% in Au + Au collisions at  $\sqrt{s_{NN}} = 200$  GeV. STAR experiment data [58] are also shown.

( $N_{\text{part}}$ ) in HYDJET ++ calculations while in experimental results mean  $p_T$  decreases with decreasing  $N_{\text{part}}$  value.

The enhancement in particle ratios at intermediate  $p_T$  may be possible due to the recombination of a shower parton from a jet with in-medium emitted thermal parton [57]. Few models [70] utilize the recombination mechanism to successfully describe enhancement in particle ratios at intermediate  $p_T$  at RHIC energy. The EPOS model [33], which contains both soft and hard physics, reproduces the enhancement in particle ratios at intermediate  $p_T$  from central to peripheral events at LHC energy by incorporating the interaction between bulk matter and quenched jets [59,69]. However, in HYDJET ++, the partons produced in (semi-) hard processes with the momentum transfer lower than  $p_T^{\text{min}}$  (an input parameter of the model) are considered as thermalized and their hadronization products are included in the soft part of the

event. The interaction between jet parton and in-medium emitted parton is not considered. This may be the possible reason why HYDJET ++ reproduces the shape of the particle ratios at intermediate  $p_T$  but not the scale of enhancement. The same issue with the model has been pointed out in Ref. [72] while analyzing the elliptic flow correlations at low and high  $p_T$  in Pb + Pb collisions at  $\sqrt{s_{NN}} = 5.02$  TeV. It has been suggested to improve the model in the intermediate  $p_T$  region by incorporating minijet production or some other mechanism.

Figures 18 and 19 show  $p_T$  integrated ratios of identified hadrons over  $\pi$ ,  $K$ , and  $K_s^0$  as a function of centrality for Au + Au and Pb + Pb collisions, respectively. For comparing the model results with experimental data, the results of the STAR Collaboration [55,58,66] for Au + Au collisions and the ALICE Collaboration [21,60,67] for Pb + Pb collisions are also shown. The strange-to-nonstrange hadron ratios are

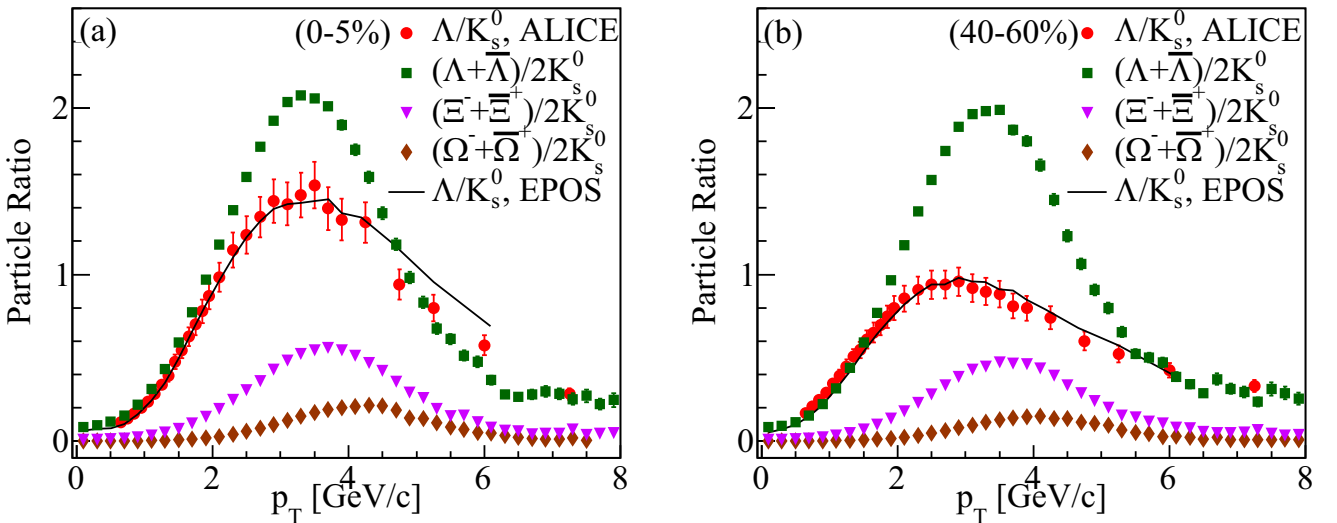


FIG. 17. Strange hadron to  $K_s^0$  ratio as a function of  $p_T$  for centrality interval (a) 0–5% and (b) 40–60% in Pb + Pb collisions at  $\sqrt{s_{NN}} = 2.76$  TeV. ALICE data [60] are also shown.



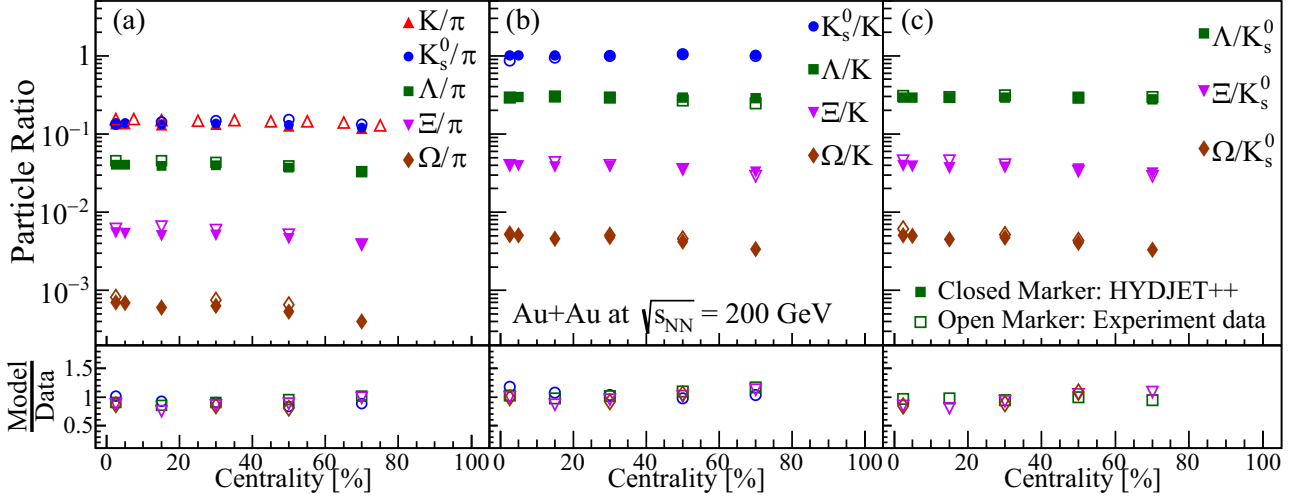


FIG. 18. Particle ratio as a function of centrality in Au + Au collisions at  $\sqrt{s_{NN}} = 200$  GeV. Solid markers represent HYDJET++ results while open markers represent STAR experiment data [55,58,66].

sensitive to the details of chemical freezeout [73]. Comparing  $p_T$  integrated strange-to-nonstrange hadron ratios with the experimental data in Figs. 18(a) and 19(b), it can be seen that the model calculations match well with the experimental data for singly strange hadrons. For multistrange hadrons, the model underestimates the experimental data. It may indicate that the chemical equilibrium is achieved in the model for singly strange hadrons but not for multistrange hadrons, especially for Pb + Pb collisions where a large deviation between model and experiment is observed for  $\Xi/\pi$  and  $\Omega/\pi$  ratios. From Figs. 18(b) and 18(c) and Figs. 19(b) and 19(c), it can be observed that the model result for particle ratios matches with the experimental data for all the centrality intervals in Au + Au collisions. However, the model underpredicts the experimental data for  $\Omega$ -to-meson ratios in Pb + Pb collisions. It is interesting to note that  $p_T$  differential ratios are not reproduced by the model in the intermediate  $p_T$  region, where it overpredicts the experimental result for  $\Lambda$ -to-meson ratios

while in the high- $p_T$  region, the model underpredicts the experimental data for the kaon-to-pion ratios. The  $p_T$  integrated ratios are well reproduced by the model apart from  $\Omega$  ratios in Pb + Pb collisions. This indicates that the integrated yields are dominated by low- $p_T$  particles, implying that the particle multiplicities are well described by HYDJET++.

### C. Strangeness enhancement factor

The strangeness enhancement factor may be defined as:

$$E(i) = \frac{\text{Yield}^{AA}(i)/\langle N_{\text{part}}^{AA} \rangle}{\text{Yield}^{NN}(i)/\langle N_{\text{part}}^{NN} \rangle}, \quad (3)$$

where  $\langle N_{\text{part}} \rangle$  is the average number of participants.  $\langle N_{\text{part}} \rangle$  and integrated yield at midrapidity obtained from the HYDJET++ model are summarized in Table I for Au + Au collisions at  $\sqrt{s_{NN}} = 200$  GeV and in Table II for Pb + Pb collisions at  $\sqrt{s_{NN}} = 2.76$  TeV.

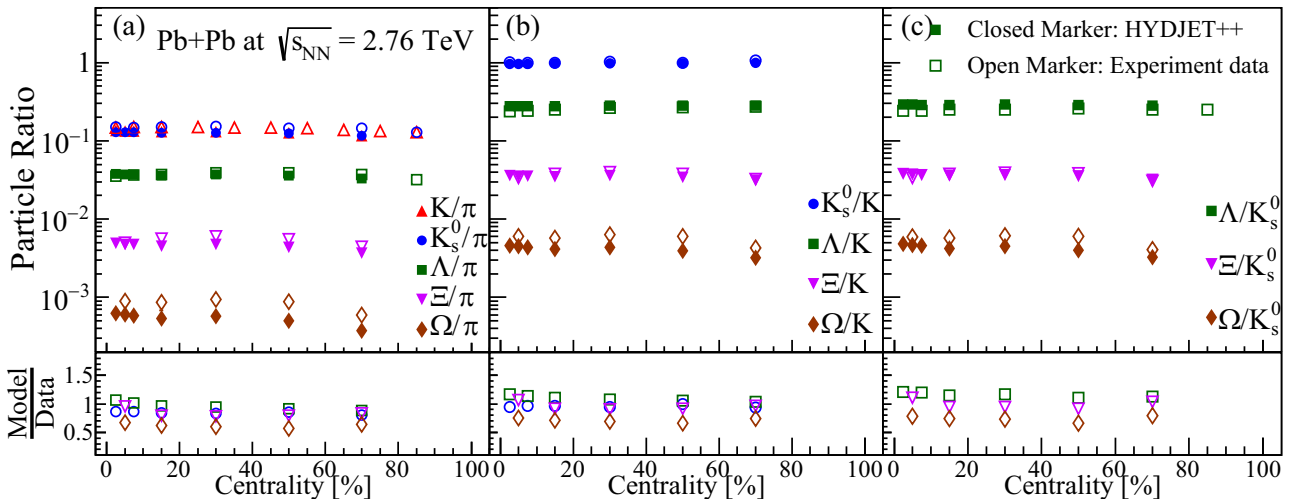


FIG. 19. Particle ratio as a function of centrality in Pb + Pb collisions at  $\sqrt{s_{NN}} = 2.76$  TeV. Solid markers represent HYDJET++ results while open markers represent ALICE experiment data [21,60,67].

TABLE I.  $\langle N_{\text{part}} \rangle$  and integrated  $dN/dy$  at midrapidity for Au+Au collisions at  $\sqrt{s_{NN}} = 200$  GeV from HYDJET++ model.

Centrality ( $N_{\text{part}}$ )	0–5%	0–10%	10–20%	20–40%	40–60%	60–80%
$\langle N_{\text{part}} \rangle$	346.16	317.28	223.86	129.35	51.80	14.25
$\Lambda$	$13.759 \pm 0.059$	$12.435 \pm 0.056$	$8.173 \pm 0.037$	$4.759 \pm 0.022$	$1.715 \pm 0.009$	$0.411 \pm 0.003$
$\bar{\Lambda}$	$11.002 \pm 0.052$	$9.939 \pm 0.050$	$6.519 \pm 0.033$	$3.789 \pm 0.020$	$1.360 \pm 0.008$	$0.324 \pm 0.003$
$\Xi^-$	$1.801 \pm 0.024$	$1.614 \pm 0.023$	$1.025 \pm 0.015$	$0.602 \pm 0.009$	$0.207 \pm 0.004$	$0.046 \pm 0.001$
$\bar{\Xi}^+$	$1.506 \pm 0.022$	$1.357 \pm 0.021$	$0.859 \pm 0.014$	$0.504 \pm 0.008$	$0.172 \pm 0.003$	$0.038 \pm 0.001$
$\Omega^- + \bar{\Omega}^+$	$0.434 \pm 0.012$	$0.385 \pm 0.011$	$0.232 \pm 0.007$	$0.139 \pm 0.004$	$0.044 \pm 0.002$	$0.0087 \pm 0.0005$

Figures 20 and 21 show strangeness enhancement  $E(i)$  as a function of the mean number of participants  $\langle N_{\text{part}} \rangle$  in Au + Au collisions at  $\sqrt{s_{NN}} = 200$  GeV and Pb + Pb collisions at  $\sqrt{s_{NN}} = 2.76$  TeV, respectively. For the present study, the  $p + p$  data of the STAR experiment [74] at  $\sqrt{s_{NN}} = 200$  GeV is used for enhancement factor calculation. The  $p + p$  data at  $\sqrt{s_{NN}} = 2.76$  TeV is evaluated using the procedure mentioned in the ALICE experiment article [21]. The  $E(i)$  for strange baryons are presented in Figs. 20(a)  $\Lambda$ , 20(b)  $\bar{\Lambda}$ , 20(c)  $\Xi^-$ , 20(d)  $\bar{\Xi}^+$ , and 20(e)  $\Omega^- + \bar{\Omega}^+$ , respectively. The STAR experiment data [22] of  $E(i)$  as function of  $\langle N_{\text{part}} \rangle$  for various strange baryons is also shown to compare with the HYDJET++ model results. The published results of strangeness enhancement from UrQMD, AMPT, and HIJING models taken from Ref. [75] are also presented for various strange baryons. It can be seen that the enhancement ratio obtained by the model show dependence on  $N_{\text{part}}$  and increases with increase in  $N_{\text{part}}$  as observed in experimental data. The enhancement ratios are well within the experimental errors in peripheral collisions. However, toward central collisions the model underestimates the experimental data. The trend of increase in the enhancement ratio with the increase in strange valence (anti-) quarks is also correctly reproduced by HYDJET++. All other simulation models, shown in Fig. 20, fail to describe the strangeness enhancement and the mass hierarchy. For Pb + Pb collisions at 2.76 TeV in Fig. 21, the strangeness enhancement is observed for (multi-)strange hadrons. However, the model result for the  $\Omega$  baryon does not scale with the experimental results. The trend of the decrease in enhancement values with increasing center-of-mass energy is observed in the HYDJET++ results which is in accordance with experimental observations [21,76]. The enhancement in Au + Au collisions at 200 GeV is higher in comparison with Pb + Pb collisions at  $\sqrt{s_{NN}} = 2.76$  TeV. It can also be seen that the scale of enhancement for baryon and

antibaryon ( $\Xi^-$  and  $\bar{\Xi}^+$  in Fig. 21) obtained from HYDJET++ is the same because of the vanishing net-baryon number at the LHC energy regime. This observation is in agreement with the ALICE experiment results. However, we observe a difference in the scale of enhancement for baryon and antibaryon ( $\Lambda$ ,  $\bar{\Lambda}$ ,  $\Xi^-$ , and  $\bar{\Xi}^+$  in Fig. 20) because of the finite net-baryon number at RHIC energy. The enhancement values for antibaryons are lower in comparison with the corresponding baryons.

#### IV. CONCLUSION

We have studied the production of strange and multi-strange hadrons in Au + Au collisions at  $\sqrt{s_{NN}} = 200$  GeV and in Pb + Pb collisions at  $\sqrt{s_{NN}} = 2.76$  TeV using the HYDJET++ model. We have calculated  $p_T$  spectra of (multi-) strange hadrons and observed that HYDJET++ generally describes the transverse momentum spectra of  $K$ ,  $K_s^0$ ,  $\Lambda$ ,  $\Xi$ , and  $\Omega$  from low  $p_T$  (soft part) and high  $p_T$  (hard part) at both RHIC and LHC energies. We observed that strange quark thermalization might not be achieved for massive strange baryons ( $\Xi$  and  $\Omega$ ) toward peripheral collisions. We have reported the particle ratios as a function of  $p_T$  in 0–5% and 40–60% centrality interval and observed that antiparticle-to-particle ratios support the experimental result of nonvanishing baryon chemical potential at RHIC and vanishing baryon chemical potential at LHC energy. We found that  $p_T$  differential ratios of  $K$ ,  $K_s^0$ ,  $\Lambda$ ,  $\Xi$ , and  $\Omega$  to  $\pi$ ,  $K$ , and  $K_s^0$  show strong dependence on  $p_T$  while no centrality dependence at both the energies. We observe that peak maximum of the particle ratios shift toward high  $p_T$  and simultaneously decreases with an increase in valence strange (anti-) quark content in hyperons. The  $p_T$  integrated ratios match well with the experimental data apart from  $\Omega$ -to-meson ratios in Pb + Pb collisions. Strange-to-nonstrange hadron

TABLE II.  $\langle N_{\text{part}} \rangle$  and integrated  $dN/dy$  at midrapidity for Pb+Pb collisions at  $\sqrt{s_{NN}} = 2.76$  TeV from HYDJET++ model.

Centrality ( $N_{\text{part}}$ )	0–5%	0–10%	5–10%	10–20%	20–40%	40–60%	60–80%
$\langle N_{\text{part}} \rangle$	374.69	343.75	315.70	242.53	139.86	55.40	14.23
$\Lambda$	$30.112 \pm 0.142$	$26.792 \pm 0.134$	$24.212 \pm 0.127$	$17.478 \pm 0.094$	$9.976 \pm 0.050$	$3.499 \pm 0.019$	$0.771 \pm 0.006$
$\bar{\Lambda}$	$30.091 \pm 0.142$	$26.793 \pm 0.134$	$24.195 \pm 0.127$	$17.470 \pm 0.094$	$9.961 \pm 0.050$	$3.498 \pm 0.019$	$0.770 \pm 0.006$
$\Xi^-$	$3.892 \pm 0.051$	$3.434 \pm 0.048$	$3.081 \pm 0.045$	$2.175 \pm 0.033$	$1.262 \pm 0.018$	$0.424 \pm 0.007$	$0.087 \pm 0.002$
$\bar{\Xi}^+$	$3.887 \pm 0.051$	$3.430 \pm 0.048$	$3.084 \pm 0.045$	$2.174 \pm 0.033$	$1.259 \pm 0.018$	$0.426 \pm 0.007$	$0.087 \pm 0.002$
$\Omega^- + \bar{\Omega}^+$	$0.996 \pm 0.026$	$0.866 \pm 0.024$	$0.767 \pm 0.023$	$0.517 \pm 0.016$	$0.307 \pm 0.009$	$0.098 \pm 0.003$	$0.0178 \pm 0.0009$

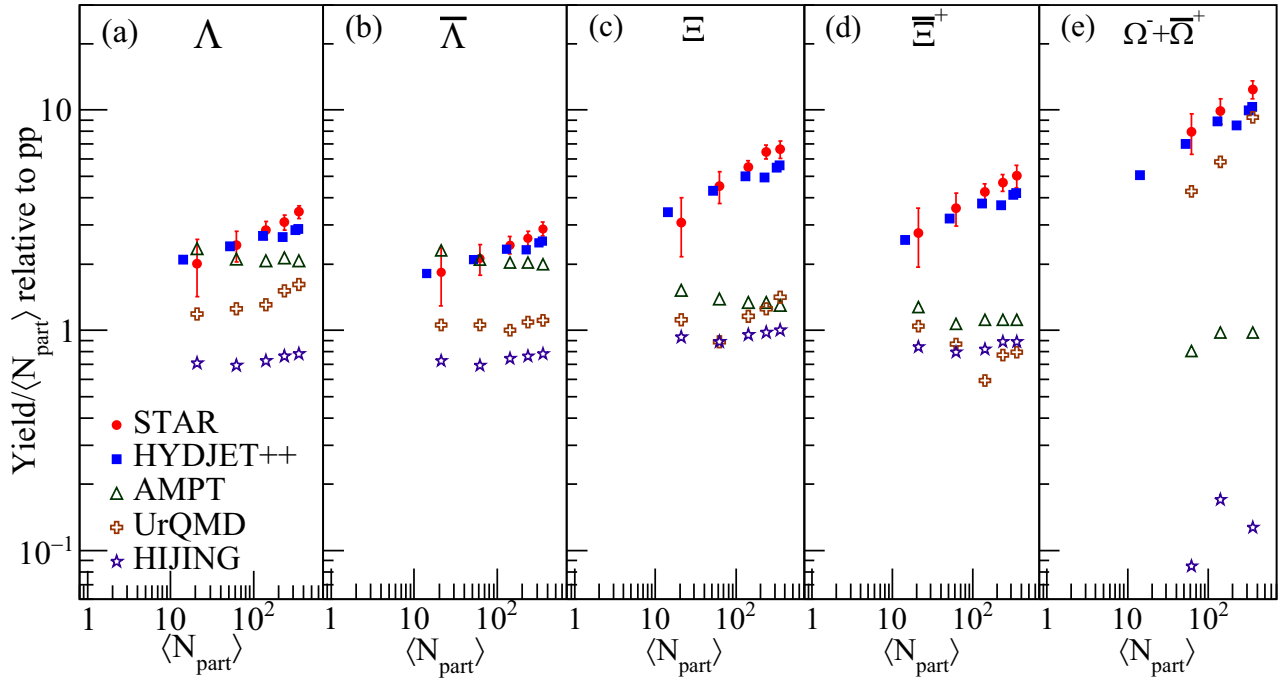


FIG. 20. Strangeness enhancement  $[E(i)]$  as a function of the mean number of participants  $\langle N_{\text{part}} \rangle$  in (a)  $\Lambda$ , (b)  $\bar{\Lambda}$ , (c)  $\Xi^-$ , (d)  $\bar{\Xi}^+$ , and (e)  $\Omega^- + \bar{\Omega}^+$  in Au + Au collisions at  $\sqrt{s_{NN}} = 200$  GeV. STAR experiment data [22] are also shown.

ratios suggest that the model achieves chemical equilibrium for singly strange hadrons but not for multistrange hadrons ( $\Xi$  and  $\Omega$ ). Further, we have calculated the strangeness enhancement factor as a function of  $\langle N_{\text{part}} \rangle$  at both RHIC and

LHC energies. We observed that the enhancement ratio obtained from HYDJET++ increases with  $\langle N_{\text{part}} \rangle$  as observed in various experiments. HYDJET++ calculations show an increase in the enhancement value with the increase in num-

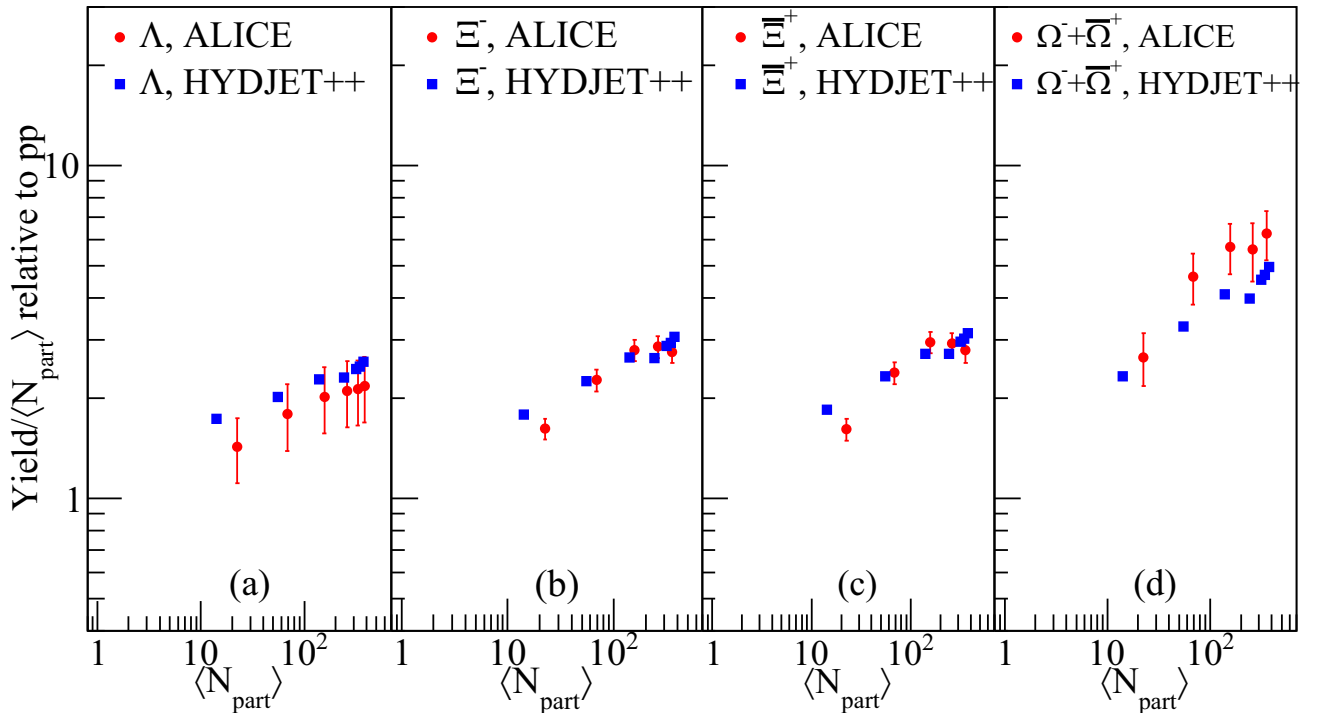


FIG. 21. Strangeness enhancement  $[E(i)]$  as a function of the mean number of participants  $\langle N_{\text{part}} \rangle$  in (a)  $\Lambda$ , (b)  $\Xi^-$ , (c)  $\bar{\Xi}^+$ , and (d)  $\Omega^- + \bar{\Omega}^+$  in Pb + Pb collisions at  $\sqrt{s_{NN}} = 2.76$  TeV. ALICE experiment data [21,76] are also shown.

ber of valence strange (anti-) quark at both RHIC and LHC energies. Other simulation models such as UrQMD, AMPT, and HIJING fail to describe the mass hierarchy in strangeness enhancement observed at RHIC.

Finally, we may conclude that the HYDJET++ provides overall a good description of strangeness production in high-energy heavy-ion collisions. Moreover, it is necessary to further improve the description of the bulk matter and incorporate the interaction between medium and jet partons to address the enhancement in baryon-to-meson ratios at intermediate  $p_T$ . The strangeness production from Pythia should be improved by incorporating reduction mechanism for strange quark suppression. Strange particle production from the soft part may be further improved by including

diquark and strange diquark suppression factors. We will focus on these issues in our future work.

#### ACKNOWLEDGMENTS

The authors thank Professor I. P. Lokhtin for useful discussions and providing expertise in the technical issues. B.K.S. gratefully acknowledges the financial support provided by the BHU Institutions of Eminence (IoE) Grant No. 6031, Government of India. A.S. thanks CSIR, India, for providing Senior Research Fellowship (Award No. 09/0013(11415)/2021-EMR-I). G.D. acknowledges the financial support obtained from UGC under research fellowship scheme in central universities.

- 
- [1] J. Rafelski and B. Müller, *Phys. Rev. Lett.* **48**, 1066 (1982).  
 [2] P. Koch, B. Müller, and J. Rafelski, *Phys. Rep.* **142**, 167 (1986).  
 [3] C. Blume and C. Markert, *Prog. Part. Nucl. Phys.* **66**, 834 (2011).  
 [4] J. Adam *et al.* (ALICE Collaboration), *Nat. Phys.* **13**, 535 (2017).  
 [5] S. Margetis, K. Safarik, and O. V. Baillie, *Annu. Rev. Nucl. Part. Sci.* **50**, 299 (2000).  
 [6] J. Schwinger, *Phys. Rev.* **82**, 664 (1951).  
 [7] M. Bleicher, W. Greiner, H. Stöcker, and N. Xu, *Phys. Rev. C* **62**, 061901(R) (2000).  
 [8] A. V. Prozorkevich, S. A. Smolyansky, V. V. Skokov, and E. E. Zabrodin, *Phys. Lett. B* **583**, 103 (2004).  
 [9] I. Arsene *et al.* (BRAHMS Collaboration), *Nucl. Phys. A* **757**, 1 (2005).  
 [10] B. B. Back *et al.* (PHOBOS Collaboration), *Nucl. Phys. A* **757**, 28 (2005).  
 [11] J. Adams *et al.* (STAR Collaboration), *Nucl. Phys. A* **757**, 102 (2005).  
 [12] K. Adcox *et al.* (PHENIX Collaboration), *Nucl. Phys. A* **757**, 184 (2005).  
 [13] J. Schaffner-Bielich, *J. Phys. G: Nucl. Part. Phys.* **30**, R245 (2004).  
 [14] S. Mrowczynski, *Acta Phys. Pol. B* **37**, 427 (2006).  
 [15] C. Greiner and S. Leupold, *J. Phys. G: Nucl. Part. Phys.* **27**, L95 (2001).  
 [16] J. Kapusta and I. Shovkovy, *Phys. Rev. C* **68**, 014901 (2003).  
 [17] P. Huovinen and J. Kapusta, *Phys. Rev. C* **69**, 014902 (2004).  
 [18] J. Noronha-Hostler, C. Greiner, and I. A. Shovkovy, *Phys. Rev. Lett.* **100**, 252301 (2008).  
 [19] J. Noronha-Hostler, H. Ahmad, J. Noronha, and C. Greiner, *Phys. Rev. C* **82**, 024913 (2010).  
 [20] D. Zschesche, S. Schramm, J. Schaffner-Bielich, H. Stöcker, and W. Greiner, *Phys. Lett. B* **547**, 7 (2002).  
 [21] B. Abelev *et al.* (ALICE Collaboration), *Phys. Lett. B* **728**, 216 (2014).  
 [22] B. I. Abelev *et al.* (STAR Collaboration), *Phys. Rev. C* **77**, 044908 (2008).  
 [23] F. Antinori *et al.* (NA57 Collaboration), *J. Phys. G: Nucl. Part. Phys.* **32**, 427 (2006).  
 [24] F. Antinori *et al.* (NA57 Collaboration), *J. Phys. G: Nucl. Part. Phys.* **37**, 045105 (2010).  
 [25] B. Abelev *et al.* (ALICE Collaboration), *Phys. Lett. B* **728**, 25 (2014).  
 [26] Z.-W. Lin, C. M. Ko, B.-A. Li, B. Zhang, and S. Pal, *Phys. Rev. C* **72**, 064901 (2005).  
 [27] B. Zhang, C. M. Ko, B.-A. Li, and Z. Lin, *Phys. Rev. C* **61**, 067901 (2000).  
 [28] S. Pal, C. M. Ko, and Z.-W. Lin, *Nucl. Phys. A* **730**, 143 (2004).  
 [29] T. Shao, J. Chen, C. M. Ko, and Z.-W. Lin, *Phys. Rev. C* **102**, 014906 (2020).  
 [30] X.-N. Wang and M. Gyulassy, *Phys. Rev. D* **44**, 3501 (1991).  
 [31] M. Gyulassy and X.-N. Wang, *Comput. Phys. Commun.* **83**, 307 (1994).  
 [32] K. Werner, *Phys. Rev. Lett.* **98**, 152301 (2007).  
 [33] K. Werner, Iu. Karpenko, M. Bleicher, T. Pierog, and S. Porteboeuf-Houssais, *Phys. Rev. C* **85**, 064907 (2012).  
 [34] P. Bożek, *Phys. Rev. C* **85**, 034901 (2012).  
 [35] P. Bożek, *Acta Phys. Pol. B* **43**, 689 (2012).  
 [36] S. A. Bass *et al.*, *Prog. Part. Nucl. Phys.* **41**, 255 (1998).  
 [37] M. Bleicher *et al.*, *J. Phys. G: Nucl. Part. Phys.* **25**, 1859 (1999).  
 [38] X. Zhu, F. Meng, H. Song, and Y.-X. Liu, *Phys. Rev. C* **91**, 034904 (2015).  
 [39] H. Song and U. Heinz, *Phys. Lett. B* **658**, 279 (2008).  
 [40] I. P. Lokhtin, L. V. Malinina, S. V. Petrushanko, A. M. Snigirev, I. Arsene, and K. Tywoniuk, *Comput. Phys. Commun.* **180**, 779 (2009).  
 [41] I. P. Lokhtin and A. M. Snigirev, *Eur. Phys. J. C* **45**, 211 (2006).  
 [42] I. P. Lokhtin, S. V. Petrushanko, A. M. Snigirev, and C. Yu. Teplov, PoSLHC07:003 (2007) [arXiv:0706.0665].  
 [43] I. P. Lokhtin, L. V. Malinina, S. V. Petrushanko, A. M. Snigirev, I. Arsene, and K. Tywoniuk, PoS HIGH-pTLHC08:002 (2008) [arXiv:0810.2082].  
 [44] T. Sjöstrand, S. Mrenna, and P. Skands, *J. High Energy Phys.* **05** (2006) 026.  
 [45] B. Andersson, *The Lund Model* (Cambridge University Press, Cambridge, UK, 1998).  
 [46] I. P. Lokhtin and A. M. Snigirev, *Eur. Phys. J. C* **16**, 527 (2000).  
 [47] R. Baier, Yu. L. Dokshitzer, A. H. Mueller, and D. Schiff, *Phys. Rev. C* **60**, 064902 (1999).  
 [48] R. Baier, Yu. L. Dokshitzer, A. H. Mueller, and D. Schiff, *Phys. Rev. C* **64**, 057902 (2001).  
 [49] K. Tywoniuk, I. C. Arsene, L. Bravina, A. B. Kaidalov, and E. Zabrodin, *Phys. Lett. B* **657**, 170 (2007).  
 [50] A. Buckley *et al.*, *Eur. Phys. J. C* **65**, 331 (2010).  
 [51] N. S. Amelin, R. Lednicky, T. A. Pocheptsov, I. P. Lokhtin, L. V. Malinina, A. M. Snigirev, I. A. Karpenko, and Y. M. Sinyukov, *Phys. Rev. C* **74**, 064901 (2006).

- [52] N. S. Amelin, R. Lednicky, I. P. Lokhtin, L. V. Malinina, A. M. Snigirev, I. A. Karpenko, Y. M. Sinyukov, I. Arsene, and L. Bravina, *Phys. Rev. C* **77**, 014903 (2008).
- [53] G. Torrieri *et al.*, *Comput. Phys. Commun.* **167**, 229 (2005).
- [54] F. Becattini, J. Manninen, and M. Gaździcki, *Phys. Rev. C* **73**, 044905 (2006).
- [55] J. Adams *et al.* (STAR Collaboration), *Phys. Rev. Lett.* **98**, 062301 (2007).
- [56] J. Cleymans, B. Kämpfer, M. Kaneta, S. Wheaton, and N. Xu, *Phys. Rev. C* **71**, 054901 (2005).
- [57] A. Adare *et al.* (PHENIX Collaboration), *Phys. Rev. C* **88**, 024906 (2013).
- [58] G. Agakishiev *et al.* (STAR Collaboration), *Phys. Rev. Lett.* **108**, 072301 (2012).
- [59] J. Adam *et al.* (ALICE Collaboration), *Phys. Rev. C* **93**, 034913 (2016).
- [60] B. Abelev *et al.* (ALICE Collaboration), *Phys. Rev. Lett.* **111**, 222301 (2013).
- [61] H. Y. Long, S. Q. Feng, D. M. Zhou, Y. L. Yan, H. L. Ma, and B. H. Sa, *Phys. Rev. C* **84**, 034905 (2011).
- [62] R. Xiao-Wen, FENG Sheng-Qin, YUAN Xian-Bao, *Chin. Phys. C* **38**, 054102 (2014).
- [63] T. Wibig, *Eur. Phys. J. C* **74**, 2966 (2014).
- [64] X. Zhu, *Adv. High Energy Phys.* **2016**, 4236492 (2016).
- [65] Y. He and Z.-W. Lin, *Phys. Rev. C* **96**, 014910 (2017).
- [66] B. I. Abelev *et al.* (STAR Collaboration), *Phys. Rev. C* **79**, 034909 (2009).
- [67] B. Abelev *et al.* (ALICE Collaboration), *Phys. Rev. C* **88**, 044910 (2013).
- [68] X.-N. Wang, *Phys. Rev. C* **58**, 2321 (1998).
- [69] K. Werner, *Phys. Rev. Lett.* **109**, 102301 (2012).
- [70] Rudolph C. Hwa and C. B. Yang, *Phys. Rev. C* **75**, 054904 (2007).
- [71] R. Rath, S. Tripathy, R. Sahoo, S. De, and M. Younus, *Phys. Rev. C* **99**, 064903 (2019).
- [72] L. V. Bravina, G. Kh. Eyyubova, V. L. Korotkikh, I. P. Lokhtin, S. V. Petrushanko, A. M. Snigirev, and E. E. Zabrodin, *Phys. Rev. C* **103**, 034905 (2021).
- [73] S. Chatterjee and B. Mohanty, *Phys. Rev. C* **90**, 034908 (2014).
- [74] B. I. Abelev *et al.* (STAR Collaboration), *Phys. Rev. C* **75**, 064901 (2007).
- [75] N. K. Behera, R. Sahoo, and B. K. Nandi, *Adv. High Energy Phys.* **2013**, 273248 (2013).
- [76] B. Abelev *et al.* (ALICE Collaboration), *Phys. Rev. C* **91**, 024609 (2015).